

Differential roles of the fish chitinous membrane in gut barrier immunity and digestive compartments

Zirui Yue^{1,2} , Zhaoyu Fan¹, Hao Zhang¹, Buhan Feng¹, Chengyi Wu³, Shenghui Chen¹, Jihua Ouyang¹ , Huiping Fan¹ , Panwei Weng¹, Huixiong Feng¹, Shangwu Chen¹, Meiling Dong¹, Anlong Xu^{1,4,*}  & Shengfeng Huang^{1,2,**} 

Abstract

The chitin-based peritrophic matrix (PM) is a structure critical for both gut immunity and digestion in invertebrates. PM was traditionally considered lost in all vertebrates, but a PM-like chitinous membrane (CM) has recently been discovered in fishes, which may increase the knowledge on vertebrate gut physiology and structural evolution. Here, we show that in zebrafish, the CM affects ingestion behavior, microbial homeostasis, epithelial renewal, digestion, growth, and longevity. Young mutant fish without CM appear healthy and are able to complete their life cycle normally, but with increasing age they develop gut inflammation, resulting in gut atrophy. Unlike mammals, zebrafish have no visible gel-forming mucin layers to protect their gut epithelia, but at least in young fish, the CM is not a prerequisite for the antibacterial gut immunity. These findings provide new insights into the role of the CM in fish prosperity and its eventual loss in tetrapods. These findings may also help to improve fish health and conservation, as well as to advance the understanding of vertebrate gut physiology and human intestinal diseases.

Keywords barrier immunity; digestion; gut compartment; microbiota; mucosal immunity

Subject Categories Digestive System; Evolution & Ecology; Immunology

DOI 10.15252/embr.202256645 | Received 10 December 2022 | Revised 6 February 2023 | Accepted 9 February 2023 | Published online 28 February 2023
EMBO Reports (2023) 24: e56645

Introduction

The gut is the major gateway for both nutrients and harmful substances, but it is a challenge to promote digestion while avoiding harmful substances. Gut compartmentalization is a common strategy to solve this dilemma (Smith & Morton, 2010; Mowat & Agace, 2014; Agace & McCoy, 2017; Brown & Esterhazy, 2021). The chitin-

based peritrophic matrix (PM) is one of the most ancient anatomical structures evolved to achieve a certain balance between efficient digestion, robust host defense, and healthy microbial ecology. In invertebrates, PM divides the gut lumen into three radial compartments: the outer space enclosed by the PM, the PM itself and the inner space between the PM and epithelia (Terra, 2001; Merzendorfer, 2011; Dishaw *et al.*, 2016; Zhu *et al.*, 2016; Nakashima *et al.*, 2018). In insects, PM confines ingesta within the outer space, prevents it from contacting epithelia, and serves as a matrix for various proteins, including peritrophins, mucins, and enzymes (Tellam *et al.*, 1999; Hegedus *et al.*, 2009; Pais *et al.*, 2018).

Peritrophic matrix is conserved in invertebrates but was traditionally considered lost in vertebrates. Mammals have new inventions, including an acidic stomach, gel-forming mucins (GFM), and mucosal adaptive immunity, which were hypothesized to displace the PM structure (Castro *et al.*, 2014; Nakashima *et al.*, 2018). An acidic stomach reduces the hostile microbes that enter the intestines, while allowing a more diverse beneficial microbiota in the intestines (Martinsen *et al.*, 2005; Castro *et al.*, 2014; Stumpf *et al.*, 2015). GFM-based mucus layers cover the epithelia of the stomach and intestines and are proposed to be functional PM analogues (Hegedus *et al.*, 2009). In the large intestine, there are two GFM layers. The inner layer is firm and impenetrable by microbes and other substances, while the outer layer is loose and densely colonized by commensal flora (Johansson *et al.*, 2011; Paone & Cani, 2020). The secretory IgAs concentrate in the outer GFM layer, conferring delicate, adaptive immunity to shape the microbial diversity (Rogier *et al.*, 2014; Bunker & Bendelac, 2018).

Basal vertebrate fish also have GFMs, adaptive immunity and an acidic stomach (Gomez *et al.*, 2013; Jevtov *et al.*, 2014; Currie & Evans, 2020), and are commonly used models for mammalian gut biology (Kamareddine *et al.*, 2020; Lee *et al.*, 2021). Recently, two ground-breaking studies discovered that fish can produce a chitinous membrane (CM) in the gut (Tang *et al.*, 2015; Nakashima *et al.*, 2018). This changes the traditional view of the PM being lost in

¹ Guangdong Key Laboratory of Pharmaceutical Functional Genes, Southern Marine Science and Engineering Guangdong Laboratory (Zhuhai), State Key Laboratory of Biocontrol, School of Life Sciences, Sun Yat-sen University, Guangdong, China[#]

² Laboratory for Marine Biology and Biotechnology, Qingdao National Laboratory for Marine Science and Technology, Qingdao, China

³ State Key Laboratory of Cellular Stress Biology, Innovation Center for Cell Signaling Network, School of Life Sciences, Xiamen University, Xiamen, China

⁴ School of Life Sciences, Beijing University of Chinese Medicine, Beijing, China

*Corresponding author. Tel: +86 020 39332958; E-mail: lssx@mail.sysu.edu.cn

**Corresponding author. Tel: +86 020 39332958; E-mail: hshengf2@mail.sysu.edu.cn

[#]Correction added on 5 April 2023, after first online publication: Affiliation 1 has been updated.

vertebrates and raises the question about using the fish models for mammalian gut diseases.

On the contrary, fishes are the most thriving clade of vertebrates, accounting for approximately 50% of vertebrate species and approximately 70% of vertebrate biomass, and have adapted to very different environments and food habits (Nelson *et al*, 2016; Bar-On *et al*, 2018; Currie & Evans, 2020). However, currently, the fish gut is threatened by increasing pathogens, water pollution, and drastic changes in food sources, which may all be exacerbated by climate change (Austin, 1998; Portner & Peck, 2010; Fernandes *et al*, 2013; Townhill *et al*, 2017; A Maureaud *et al*, 2021; Kibria *et al*, 2021; Pepi & Focardi, 2021; Yang *et al*, 2021). In addition, alternative diets used in fish farming affect the gut health of cultured fish (Serra *et al*, 2021). Therefore, the study of the CM helps to understand the CM contribution to the fitness of fish.

The invertebrate PM is essential for digestion and immunity (Terra, 2001; Bolognesi *et al*, 2008; Hegedus *et al*, 2009). In fact, temporary and partial PM disruptions were shown to be enough to compromise invertebrate gut immunity (Edwards & Jacobs-Lorena, 2000; Wang & Granados, 2000; Kuraishi *et al*, 2011; Kelkenberg *et al*, 2015; Rodgers *et al*, 2017; Nakashima *et al*, 2018). However, without a complete genetic PM/CM knockout model, we may not study some basic properties of the PM/CM and the functional differences between the invertebrate PM and fish CM. And we may not investigate which role of the PM/CM, that is, digestion or immunity, is more important.

Here, we created a zebrafish model genetically devoid of the CM and used it to study short-term and long-term CM functions in fish growth, health, and longevity and tried to understand the underlying mechanisms. Our findings provide new insights into several aspects, including the role of the CM in fish prosperity and diversity, CM-based strategies for fish health and conservation, causes of CM loss in tetrapod vertebrates and the application of a CM-less fish model in vertebrate gut biology.

Results

Characteristics of the zebrafish CM

Previous studies have described the fish CM with electronic microscopy and histochemistry with SNAP-tagged chitin-binding domains (SNAP-CBD) and calcofluor white (CFW; Tang *et al*, 2015; Nakashima *et al*, 2018). Here, we first repeated the histochemistry to obtain more specific results. We found that the CM could be visualized in the gut lumen in adult zebrafish (Appendix Fig S1A). This anatomical structure could be removed by chitinases (Appendix Fig S1B), confirming its chitinous nature. Analysis of a series of stained sections suggested that the CM was distributed throughout the gut lumen and formed a continuous tube-like structure, encasing the ingesta from the beginning of the intestinal bulb and escorting the excrement out of the anus (Fig 1A; Appendix Fig S2A–G). This full-length continuous CM tube could be more evidently visualized in the larval zebrafish at 7-days postfertilization (Fig 1B–D), when feeding and defecating typically begin. The first CM signal, however, could be detected in larval zebrafish as early as 4–5 dpf, when the mouth opened (Appendix Fig S3). We noticed that chitin signals arose from many epithelial cells from different places (Fig 1E and F;

Appendix Fig S4A–F). This result suggested that these epithelial cells were involved in chitin synthesis, which was corroborated by the single-cell RNA-seq data described in the next section. Irregular chitin fibers were observed to form roughly parallel, loosely associated thin CM layers (Fig 1F; Appendix Fig S4C and D) and could further stack into a thicker CM layer surrounding the digesta (Fig 1G; Appendix Fig S4E and F). The CM could be detected in larvae with or without feeding (Fig 1C and D) and in adults fed or starved for 2 days (Fig 1H and I). After starvation, the gut lumen could be filled with a CM without digesta (Fig 1I). In comparison, in some insects such as mosquitoes, the PM is only secreted after a meal (Cazares-Raga *et al*, 2014).

Genes and cells related to CM synthesis in zebrafish

Previous analysis showed that vertebrate chitin synthases (CHS) belong to the metazoan type-II CHS subfamily and were duplicated into two groups (A and B) in early vertebrate evolution (Shi *et al*, 2020). Zebrafish have four CHS genes, with *chs1* belonging to group A and *chs2-4* belonging to group B (Fig 1J). In adult zebrafish, *chs1* was exclusively and abundantly expressed in the gut, whereas *chs2-4* were distributed in other tissues (Fig 1K). The *chs1* mRNA expression remained stable in the first six gut sections (S1–S6) but sharply dropped in the last one (S7; Fig 1L). Unlike *chs2-4*, which showed substantial mRNA expression beginning on the first day of embryogenesis, *chs1* began to be expressed at 4 dpf and climbed to a high level at 5 dpf (Fig 1M–P), which coincided with the first appearance of CM signals (Appendix Fig S3) and the timing of mouth opening and intestine maturation. We reanalyzed four zebrafish gut single-cell RNA-seq datasets that are publicly available in the GEO database (Dataref: Gu *et al*, 2019). The results showed that while *chs2-4* had no expression in the gut (Appendix Fig S5), *chs1* was mostly expressed by enterocytes and most enterocytes expressed *chs1* (Fig 1Q and R). These findings suggest that the zebrafish CM was produced by CHS1 in enterocytes throughout the gut. In this sense, we proposed that the zebrafish CM is a type-I CM according to the definitions of the insect PM types. Insect PM can be produced by the whole midgut (type-I PM) or by a special region of the anterior midgut (type-II PM; Hegedus *et al*, 2009).

Genetic removal of the zebrafish CM

We inactivated the zebrafish *chs1* gene by using the CRISP/Cas9 gene editing method. Due to the outbred nature of the AB strain zebrafish, it was difficult for us to assess the off-target editing effects. To minimize potential artifacts, we generated three different populations of F₂ homozygous mutants, and after observing no visible differences among these populations, we backcrossed one of them with the wild type to produce a population of F₄ homozygous mutants (Fig 2A and B). This F₄ population and its descendants were used in the rest of this study unless otherwise specified. Visual examination showed that the adult heterozygous mutants had no visible differences from the wild types, suggesting that the *chs1* mutation tends to be recessive. The adult homozygous mutants also exhibited no external defects but appeared to be smaller than the wild types at the same age (Fig 2C–E; Appendix Fig S6). Histochemistry showed that the CM completely disappeared in both homozygous mutant larvae and adults (Fig 2F–M; Appendix Fig S7).

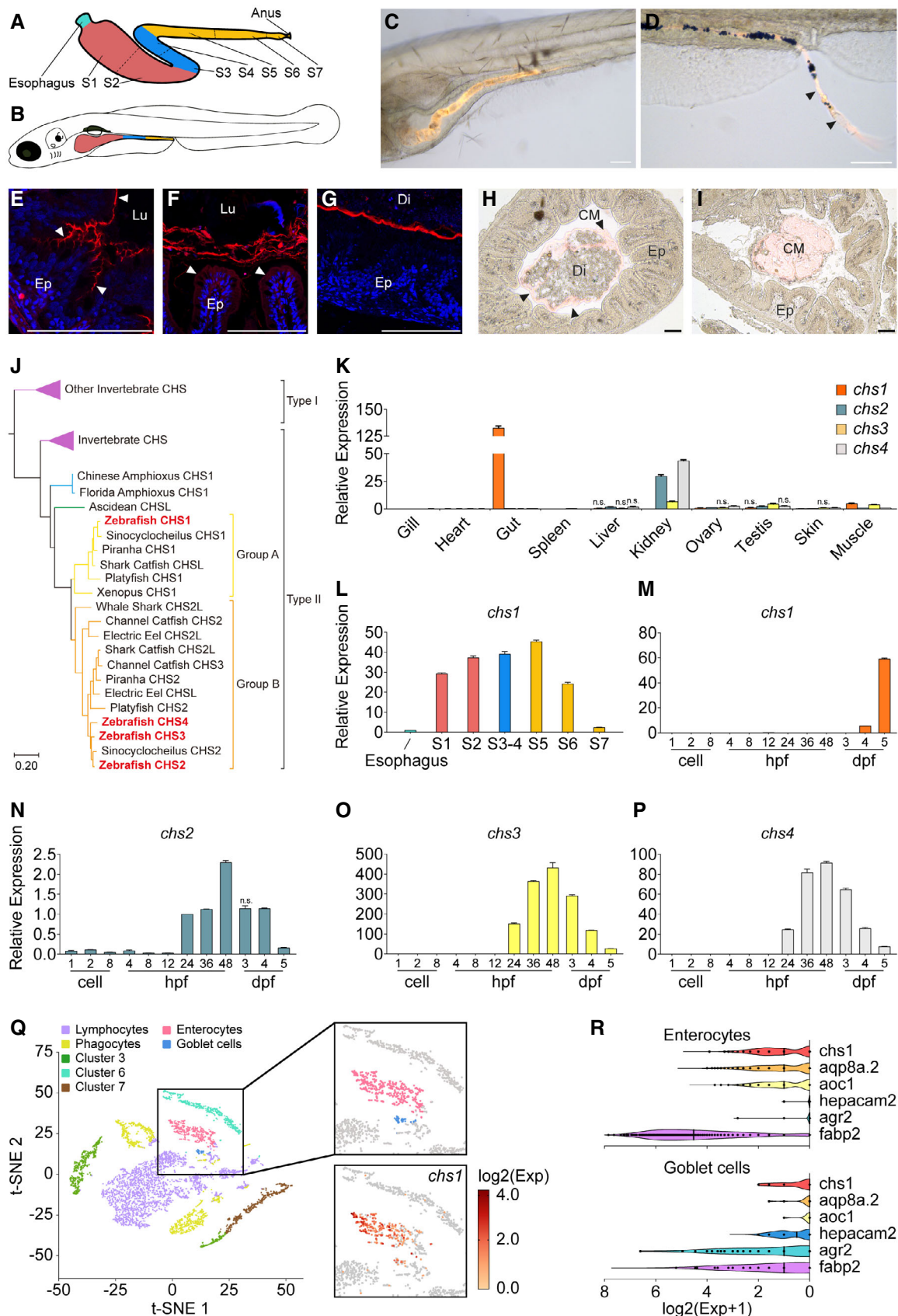


Figure 1.

Figure 1. CM characteristics in zebrafish.

- A, B The gut sections S1–S7 in adult and larva zebrafish according to previous studies (Wang *et al.*, 2010).
- C, D The CM in the 7 dpf larvae was revealed by SNAP-CBD staining. Scale bars, 100 μm. Please see Appendix Fig S3 for the images of 3–5 dpf larvae.
- E–G Newly synthesized chitin fibers (red; white triangles) from different places of the adult gut epithelia in Sections S1–S2 (E). Multiple roughly parallel CM and faint chitin signals (white triangles) on the epithelial cells in Sections S1–S2 (F). A single thick layer of CM holding the digesta away from epithelia in Sections S5–S7 (G). Red, SNAP-CBD stain; blue, DAPI stain; Ep, epithelium; Lu, lumen; Di, digesta; Scale bars, 100 μm. Please see Appendix Fig S4 for the corresponding bright-field images.
- H, I CM (black triangles) in fed adult fish with digesta and starved adult fish without digesta in the gut section S2–S4. Orange, SNAP-CBD stain; Ep, epithelium; Di, digesta; Scale bars, 50 μm.
- J Phylogenetic analysis of the type II CHS proteins in chordates, based on an early report (Shi *et al.*, 2020).
- K–P Real-time qRT–PCR revealed the expression profiles of four zebrafish *chs* genes in different tissues (K), different gut sections (L), and different developmental stages (M–P). One representative example of three repeat experiments is shown. Data were the mean ± SEM of $n = 3$ technical replicates. n.s. no significant, no label $P < 0.05$ by Student's *t*-test.
- Q Cluster map of the publicly available single-cell RNA-seq datasets showed each cell type in the gut epithelia of adult fish (here shows one of the four datasets; Dataref: Gu *et al.*, 2019). The *chs1* genes were predominantly expressed by enterocytes.
- R Violin plots (with median line) showing the selected marker genes differentially expressed in the enterocytes and goblet cells from (Q). Individual data points for each cell were plotted as black dots. Please see Appendix Fig S5 for the expression patterns of all selected marker genes.

Source data are available online for this figure.

Long-term effects of CM loss on growth, nutrition, and longevity

Chitinous membrane-less mutants were viable and fertile and had no maturation delays, behavior anomalies or external defects (Figs 2E, 3G, and 8C; Appendix Fig S6). To our surprise, in five independent experiments, mutant larvae consistently showed higher survival rates than wild-type larvae in the first 8 days after fertilization (Fig 3A and Table EV1), although this situation was reversed in juvenile and adult mutants (Fig 3B and Table EV1). This finding might be related to immunity or nutrition savings, but the actual causes need investigation. The juvenile and adult mutants showed higher mortality rates than those of the wild types (Fig 3B; Table EV1). We recorded an individual's genotype, body length, and weight from a 6-month-old F₂ population (Fig 2B), which showed that the homozygous mutants were smaller than the heterozygous mutants and wild-type fish (Fig 3C). The slow growth rates of mutants were confirmed by head-to-head comparison between mutants and wild types (Fig 3D and E; Table EV2). The difference continued to widen as the age increased, so wild-type fish had on average twice the weight of mutants at the sixth month (Fig 3E; Table EV2). Many deceased mutants suffered from weight loss and liver and gut atrophy (Fig 3F–M), which resembled the symptoms of long-term starvation (as shown in Appendix Fig S8A and B). In fact, many mutants older than 6 months began to show signs of emaciation and gut atrophy and stopped feeding for days before death. These findings suggest that the loss of the CM has age-dependent negative impacts on zebrafish.

CM loss affects gut and ingestive behavior

The CM-less zebrafish allowed us to observe for the first time how the CM changes gut behavior. In the CM-less gut of adult fish, we noticed that there was no clear boundary between the digesta and epithelia and that there was direct contact between the digesta and epithelia (Appendix Fig S7D–F). Behavior of the gut and ingestia was visualized in the larvae fed 6-μm plastic beads. Live imaging showed that wild-type larvae usually did not ingest too many beads (Fig 4A–D), but even if they ingested a large quantity of beads, the intestinal bulb still maintained plenty of space (Fig 4B). Mutant

larvae more often had excessive beads in the gut, and the bead cord expanded, jammed the whole intestinal bulb, and pressed against the epithelia (Fig 4E–H). Moreover, in mutants, the bead cord tended to have a rugged border (Fig 4E–H), and beads often escaped the bead cord and stuck between the villi, even if there were only a few beads (Fig 4E, G, I and J).

The dynamics of gut and ingestia movements were also captured in motion pictures. In wild-type fish, beads were packed into a relatively rigid cord in the intestinal bulb, and even when many beads were consumed, they could not fill up the lumen of the intestinal bulb (Movie EV1A). In wild-type fish, the wave-like movements of the gut wall pushed the cord toward the anal direction. However, in mutants, beads often jammed the whole lumen and adhered to the epithelia, making the movement of the bead cord sluggish or inefficient (Movie EV1B). Moreover, instead of steadily moving forwards as a whole as in wild types, the bead cord in mutants could be difficult to move forwards for a while and then suddenly snapped off in the middle and pulled forwards away like a rubber band (Movie EV1C). Wild-type fish excreted a rigid bead cord out of the anus by one or two pushes, while mutants slowly squeezed out a soft bead cord (Movie EV2A and B). In wild types, the relative positions of the beads were not changed much by gut movements, whereas in mutants, beads drifted more randomly (Movie EV3A and B). These observations suggest that the CM-less gut could not effectively compact, confine, and immobilize the ingestia or facilitate its movements.

The CM enhances the radial gradient of the gut microbiota

The fish gut harbors a rich indigenous community of microbes (Colston & Jackson, 2016; Lescak & Milligan-Myhre, 2017; Tarnecki *et al.*, 2017). Since fish CM divides the gut lumen into three radial compartments, it may influence the radial gradient of the gut microbial community. We dissected the zebrafish gut into two parts, the digesta and the epithelia (dissection shown in Appendix Fig S9A–C). These two parts should represent different niches for microbiota and have different bacterial compositions (Fig 5A). We separated these two parts from each 3-month-old fish and subjected them to 16S-rRNA sequencing. A total of 12 wild types and 12 mutants were sampled, and 56 16S-rRNA libraries were sequenced, which

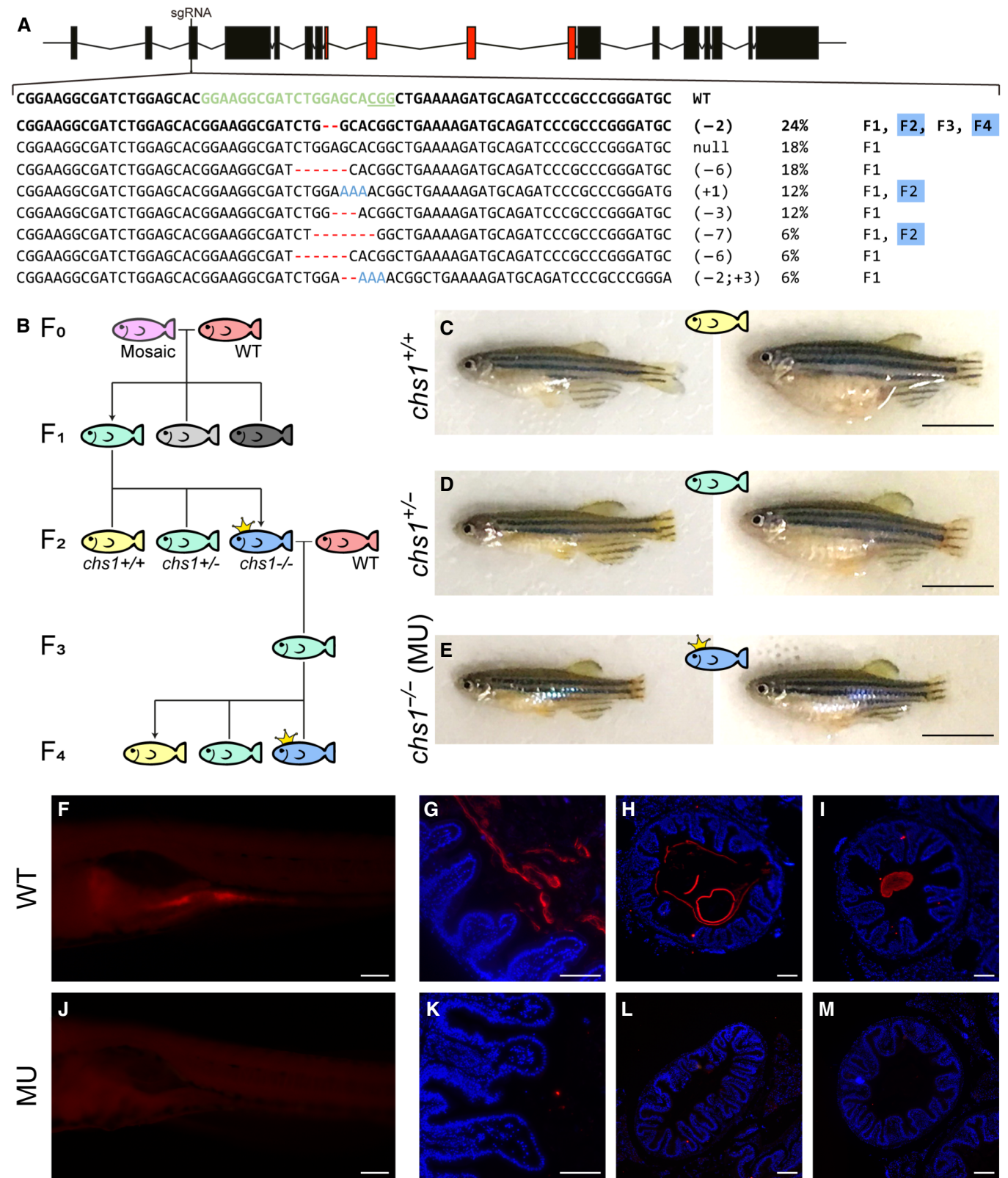


Figure 2.

Figure 2. Knockout of *chs1* causes CM loss.

- A, B The mutations and the breeding scheme. F₂ and F₄ generation of homozygous *chs1*^{-/-} mutants (in blue) were used for experiments. Different color represented different genotype.
- C–E Representatives of 6-month-old males (left) and females with developed gonads (right) belong to three different genotypes (*chs1*^{+/+}, *chs1*^{+/-} and *chs1*^{-/-}). Scale bars, 1 cm.
- F–M Compared with wild types (F–I), mutants (J–M) completely lost the CM (red) in the gut of 7dpf larva (F, J), as well as in the intestinal bulb (G, K), middle intestine (H, L) and posterior intestine (I, M) of adults. Red, SNAP-CBD stain; blue, DAPI stain; WT, wild-type; MU, *chs1*^{-/-} mutant. Scale bars, 100 μm.

Source data are available online for this figure.

included feeding/no-feeding treatments, different gut sections (S1–S7 or S2–S6 or S3–S6), and different batches (Dataset EV1). The pairwise bacterial compositional dissimilarity between the digesta (niche1) and the epithelia (niche2) was calculated for each animal on four taxonomy levels using the Jaccard distance metric (Dataset EV1). Both wild-type and mutant fish maintained a digesta-versus-epithelia difference (Fig 5B; Appendix Fig S10). However, the digesta-versus-epithelia differences were significantly higher in the wild types than in the mutants (Fig 5B; Appendix Fig S10). This result indicates that the presence of the CM could greatly increase the radial gradient of the gut bacterial composition.

CM loss leads to gut dysbiosis

To investigate whether CM loss leads to gut dysbiosis (Fig 5A), we compared the wild-type and mutant fish that were cohoused in a small aquarium system. The 16S-rRNA libraries from six wild types and six mutants were prepared from gut sections S3–S6 (including the epithelia and the content), which received less direct influence from environmental microbes than gut sections S1–S2 (Fig 1A). The alpha diversity metrics showed that wild-type and mutant samples mainly differed in the richness of bacterial OTUs (Fig 5C and D). The beta diversity metrics showed that while wild-type samples were clustered together, mutant samples were not only divergent from wild-type samples but were also divergent from each other (Fig 5E; Appendix Fig S11). Taxonomy bar plots indicated that *Actinobacteriota*, *Acidobacteriota*, and *α-Proteobacteria* were less abundant in the mutant gut than in the wild-type gut, while *γ-Proteobacteria* was more abundant in the mutant gut than in the wild-type gut and the environment (Fig 5F). The composition at other taxonomic levels, from phylum to species, was provided in Appendix Fig S12.

To determine which taxon/OTU significantly contributed to the bacterial compositional differences between wild types and mutants, we used a conservative approach implemented in LEfSe (Segata *et al.*, 2011), which helped identify a set of differentially abundant taxa, or marker taxa, with high statistical significance (Appendix Fig S13A and B; Datasets EV2 and EV3). A simplified list of these marker taxa is shown in Fig 5G. Approximately 50% of marker taxa belonged to the abovementioned *Actinobacteriota*, *Acidobacteriota*, *α-Proteobacteria*, and *γ-Proteobacteria*. Approximately 80% of marker taxa showed significantly higher abundances in the wild types than in the mutants, many of which could be viewed as beneficial (Fig 5G; Appendix Fig S13A and B; Datasets EV2 and EV3). There were seven markers with higher abundances in the mutant gut (Fig 5G; Appendix Fig S13A and B; Datasets EV2 and EV3), of which three (*Enterobacteriales*, *Staphylococcus*, and *Chthoniobacterales*) were (opportunistic) pathogens, and two (*Euzebyales* and *Geminicocaceae*) were not usually present in the gut but were in the

environment. These findings suggest that CM-less fish could not maintain a normal gut microbiota.

CM loss alters the gut transcriptome in an age-dependent fashion

We analyzed the transcriptomes of gut sections S3–S6, which receive less direct influence from the environment (Fig 1A). Thirteen transcriptomes for 13 individual fish were sampled, including two 3-month-old healthy wild-type fish, two 3-month-old seemingly healthy mutants, five 6-month-old healthy wild-type fish, two 6-month-old seemingly healthy mutants, and two 6-month-old sick mutants with obvious symptoms of emaciation and gut atrophy. Principal component analysis identified the similarities of these transcriptomes and organized them into three groups: the 3- and 6-month-old healthy wild types, the 3- and 6-month-old seemingly healthy mutants, and the 6-month-old sick mutants (Fig 6A). Remarkably, healthy individuals were collected at different ages (3 and 6 months old) and sequenced in different batches, yet their transcriptomes were still clustered together, suggesting the stability of the transcriptome in gut sections S3–S6 under normal physiological conditions. Enrichment analyses revealed that in mutants, differentially expressed genes (DEGs) were significantly involved in digestion, the cell cycle, and immunity (Fig 6B–F; Appendix Figs S14A–F, S15A–D, S16A–D, and S17A–D; Datasets EV4–EV6). Notably, the transcriptomes of the older (6-month-old) mutants were not only divergent from those of the older (6-month-old) wild-type (Fig 6C; Appendix Fig S16A–D) but were also divergent from those of the younger (3-month-old) mutants (Appendix Figs S14F and S18A–D). This finding suggests that as CM-less fish became older, their gut transcriptome deviated more from the normal status.

CM loss causes downregulation of digestive genes

Although the 3-month-old mutants appeared healthy, their genes coding for digestive enzymes and nutrient absorption were downregulated (Fig 6B and C; Appendix Fig S15A–D; Datasets EV4 and EV5). The most prominent genes included *chia.3*, *prss3*, *amy2a*, and *apoalb* (Fig 6D; Datasets EV4 and EV5). *Chia.3* encodes a chitinase for chitin degradation, *prss3* encodes a trypsin for protein digestion, and *amy2a* encodes an amylase for hydrolysis of dietary starch and glycogen. On the contrary, *apoalb* mediates the transportation of lipids from the intestines to the bloodstream. As the mutants became older (6 months old) and sicker (emaciation and gut atrophy), more digestive genes were downregulated, and the fold changes were larger (Fig 6C and D; Appendix Figs S16A–D and S17A–D; Datasets EV4 and EV5). These findings suggest that CM loss affected the efficiency of digestion and absorption.

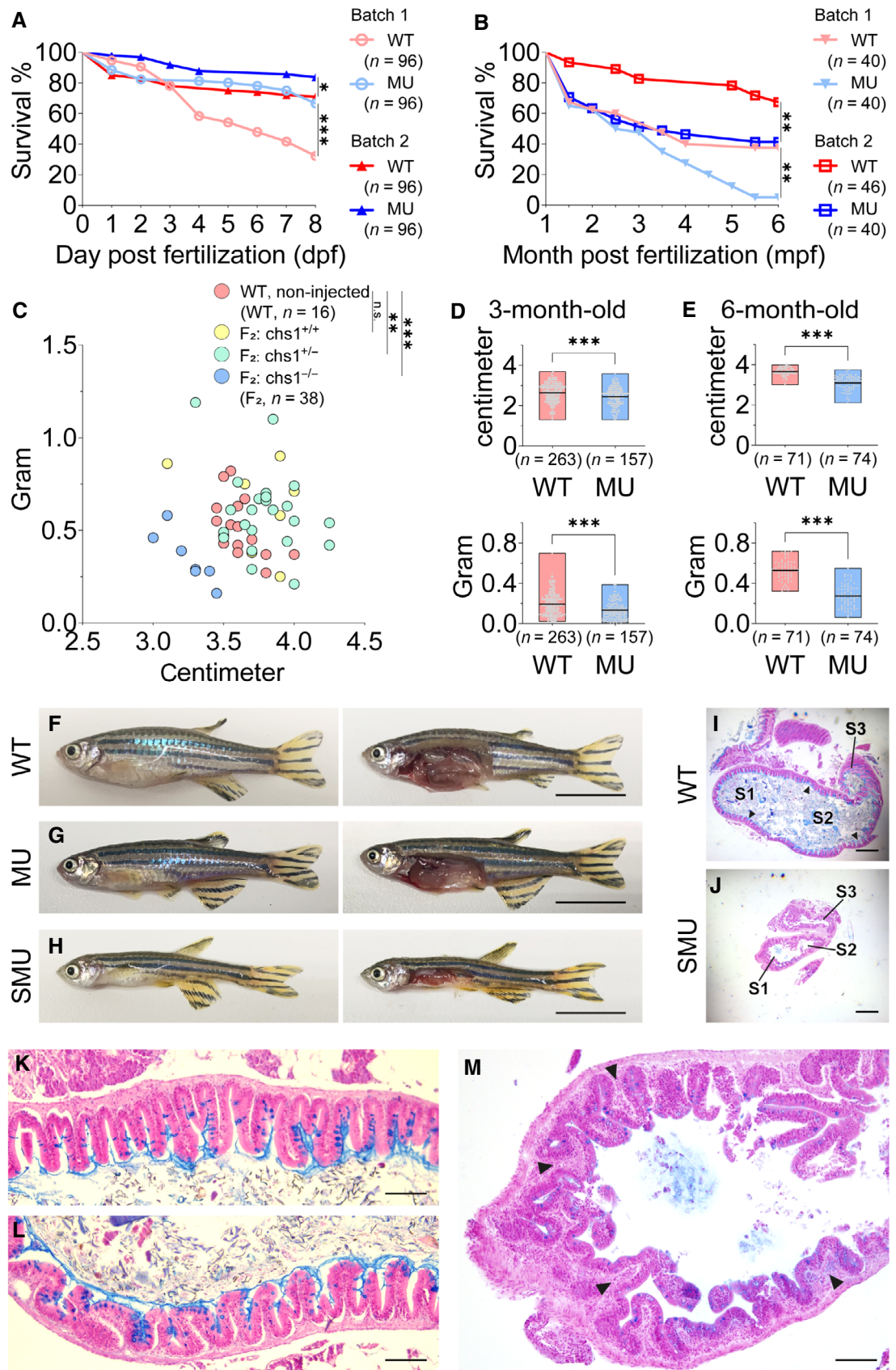


Figure 3.

Figure 3. Long-term effects of CM loss in zebrafish.

- A, B The survival rates of wild types and mutants in the first 8 days (A) and the first 6 months (B). Two independent batches (1 and 2) were conducted for each experiment. n , the initial numbers of zebrafish. * $P < 0.05$, ** $P < 0.01$, *** $P < 0.001$ by log-rank (Mantel-Cox) test. Please see Table EV1 for data on another three batches of independent experiments.
- C Plots of the genotypes, body weight, and length of the 6-month-old adult animals from an early F₂ population, as shown in Fig 2B. Noninjected wild-type adults were used as reference. n , the numbers of zebrafish. n.s. no significance, ** $P < 0.01$, *** $P < 0.001$ by one-way MANOVA test.
- D, E The body length and weight comparison in 3- or 6-month-old wild types and mutants. Data of each population were represented in box (min to max with mean line) plots. Individual data points for each animal were plotted as gray dots. n , the numbers of zebrafish. *** $P < 0.001$ by Student's t-test. Please see Table EV2 for the batch information and detailed statistics.
- F–H Comparison of the body and abdomen of the representatives of the 6-month-old wildtypes, mutants, and sick mutants. SMU, sick mutant. Scale bars, 1 cm. Please see Appendix Fig S8 to compare with the long-term starved wild-type fish.
- I, J Alcian blue staining (for mucus) and nuclear fast red staining (for nucleic acids) of the gut section S1, S2, and S3 in a 6-month-old wild-type and in a 6-month-old sick mutant. Black triangles indicate the mucus attached to the intestinal walls. Scale bars, 500 μ m.
- K, L Magnification of the wild-type gut section S1 from (I). Scale bars, 100 μ m.
- M Magnification of the sick gut section S1 from (J). Black triangles show swelling lamina propria. Scale bars, 100 μ m.

Source data are available online for this figure.

CM loss accelerates gut epithelial renewal

To withstand wear, tear, drain, and infection during digestion, the intestinal epithelia renew at a rapid pace to maintain homeostasis. Transcriptome analysis suggested that 3- and 6-month-old mutants had enhanced activities in cell cycle process, cell division, and DNA replication and repair (Fig 6B and C; Appendix Figs S15A–D and S16A–D; Datasets EV4 and EV5). The most upregulated genes included *tp53*, *ccne2*, *cdk1*, and *cdca8* (Fig 6D; Datasets EV4 and EV5). *Tp53* is a well-known tumor suppressor and stress-responsive gene for repressing and killing damaged, aged, and mutated cells. Its upregulation suggests that the gut epithelia of mutants were under damaging stress. *CCNE2* and *CDK1* encode critical components of the M-phase promoting pathway, which promote DNA synthesis and cell division. *CDCA8* is required for chromatin-induced microtubule and spindle formation during mitosis. Furthermore, compared with the 3-month-old mutants, the 6-month-old mutants had more upregulated genes associated with cell division and DNA repair but more downregulated genes related to cell migration and differentiation (Fig 6C and D; Appendix Fig S18A–D; Datasets EV4 and EV5). This result might indicate that the renewal capacity of the gut epithelia began to be exhausted in older mutants.

To verify whether epithelial repair and renewal were accelerated due to CM loss, we injected wild-type and mutant fish with bromodeoxyuridine (BrdU) and sacrificed them later for histochemistry (Fig 6E; Appendix Fig S19). With BrdU as the tracer of new cells, we found that in the mutant gut, more signal spots could be seen along the villi after 2 h, and these signal spots more quickly migrated to the villi tips after 12 h. This finding indicated that the mutant gut has excessive cell proliferation and migration activity, thereby suggesting that the CM is crucial for maintaining gut epithelial homeostasis.

Zebrafish have no visible mucin-2 layers

The large intestine of mammals is covered by a firm inner mucus layer and a loose outer mucus layer (Johansson *et al*, 2013, 2014; Paone & Cani, 2020). These layers are formed by mucin-2 and are proposed to be the functional analogues for the invertebrate PM (Hegedus *et al*, 2009; Nakashima *et al*, 2018). Zebrafish express two

mucin-2 genes (*muc2.1* and *2.4*) in the gut. We investigated whether they form into layers. In the mouse gut, we detected a firm mucus layer (blue colored; Fig 7A and B). In the gut of wild-type and mutant fish, we found pervasive mucus signals in the lumen and many mucus spots (goblet cells) in the epithelia (Fig 7C and E), but failed to detect any loose or firm mucus layers. We then conducted histochemistry with polyclonal antibodies against zebrafish mucin-2.1/2.4, which detected strong signals of mucin-2s in the goblet cells in both wild-type and mutant fish but still no visible mucin-2 layers in the lumen (green colored; Fig 7D and F). Therefore, zebrafish did not have loose or firm mucin-2 layers to protect their gut epithelia.

CM-less fish develop age-dependent inflammation

Transcriptome analysis identified many upregulated immune genes in the mutant gut (Fig 6C; Appendix Figs S16A–D, S17A–D, and S18A–D; Datasets EV4 and EV5). The prominent genes included *il17a/f3*, *cxcl11.8*, *duox*, *ttnfa*, and *il1b* (Fig 6D; Dataset EV4). In the 3-month-old mutants, both *il17a/f3* and *cxcl11.8* were already upregulated. *Il17a/f3* encodes interleukin-17, a hallmark effector of Th17 cells that mediates tissue repair and pathogen killing at the mucosal surface. *Cxcl11.8* encodes a CXCL-type chemokine capable of inducing chemotaxis in activated T cells. In the 6-month-old seemingly healthy mutants, *duox* began to be upregulated. It encodes a famous NADPH oxidase-producing ROS in the gut epithelia and is a marker of tissue repair, gut inflammation, and dysbiosis (Niethammer *et al*, 2009; Flores *et al*, 2010; Grasberger *et al*, 2015). In 6-month-old sick mutants with symptoms of gut atrophy, *ttnfa* and *il1b* were induced, which encode two hallmark pro-inflammatory cytokines (TNF α and IL-1B).

Duox may be viewed as a marker of the early stage of gut inflammation (Grasberger *et al*, 2015), whereas *ttnfa* and *il1b* are signs of severe gut inflammation. In line with this, the 6-month-old seemingly healthy mutants had more upregulated immune genes and higher upregulation levels than the 3-month-old mutants. The 6-month-old sick mutants also had more induced genes and higher induction than the 6-month-old seemingly healthy mutants (Fig 6C; Appendix Figs S17A–D and S18A–D; Datasets EV4 and EV5). Serious inflammation in the 6-month-old sick mutants was further supported by the fact that many important immune effectors were

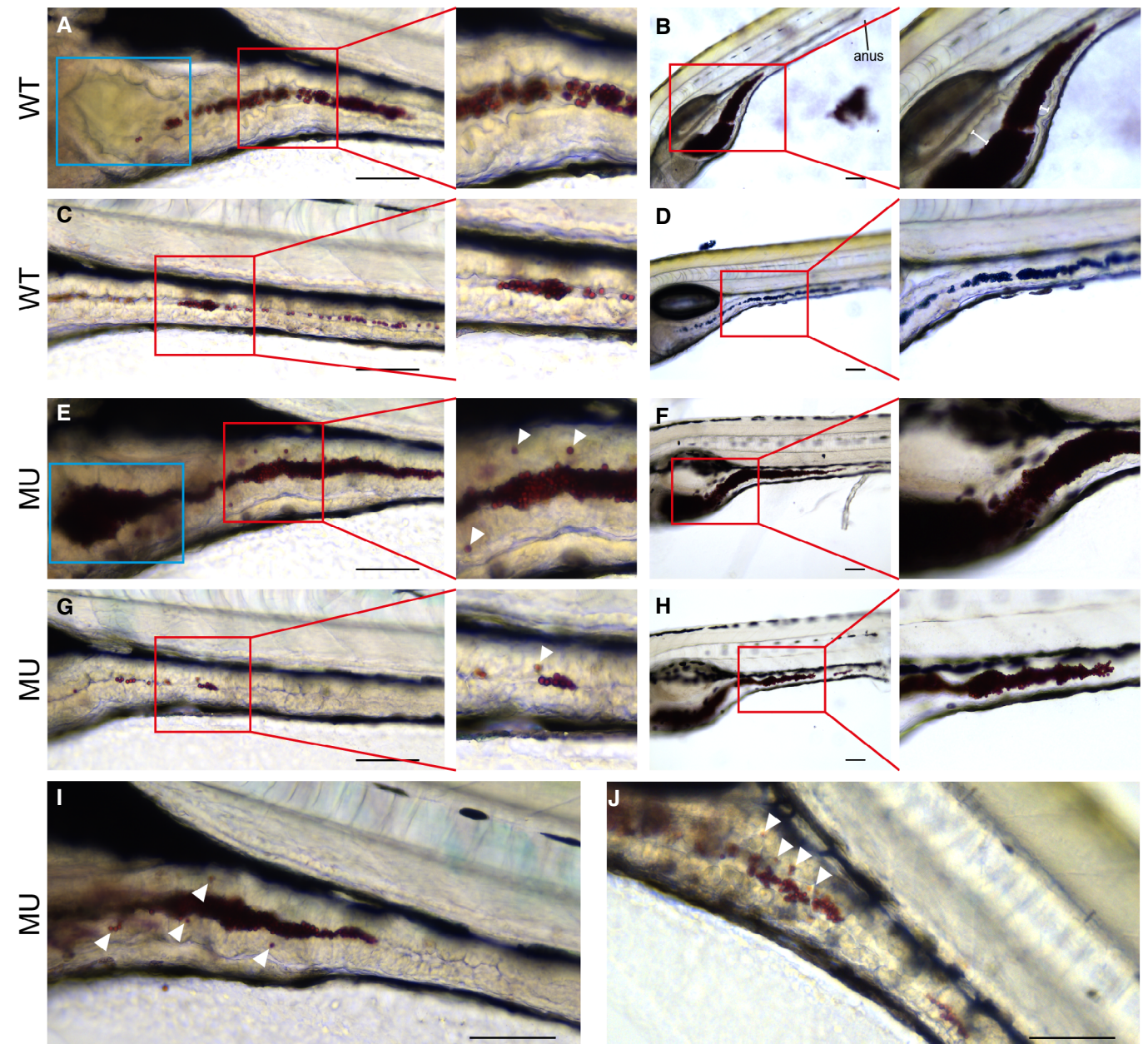


Figure 4. Gut and ingestive behavior in the larval gut without CM.

A–D 6/7 dpf larva wild types were fed with 6- μ m polystyrene beads. The beads were restricted in the bead cord and spaced from intestinal wall. Blue rectangle indicates the intestinal bulb. H-shaped bars indicate the space between digesta beads and intestinal wall. Right panels were magnification of the red rectangle area in left panels. Scale bars, 100 μ m.

E–J 6/7 dpf larva mutants were fed with 6- μ m polystyrene beads. The beads jammed in the intestinal bulb and middle intestine (E, F, H, I). In some cases, the beads escaped the bead cord and stuck between villi (white triangles; E, G, I, J). Blue rectangle indicates the intestinal bulb. Right panels were magnification of the red rectangle area in left panels. Scale bars, 100 μ m.

Source data are available online for this figure.

only significantly induced in the sick mutants but not in the seemingly healthy mutants. These include matrix metallopeptidase 9 (*mmp9*), phagocytic NADPH oxidase (*cybb/nox2*), myeloid-specific peroxidase (*mpx*), coagulation factors, and complements (Fig 6D; Dataset EV4).

Consistent with the transcriptomes, wild-type and young seemingly healthy mutants showed no obvious differences in abdomen anatomy (Fig 3F and G) and gut epithelial histochemistry (Figs 3I and 7C–F). The 6-month-old sick mutants, however, exhibited serious gut atrophy (Fig 3H, J, and M). Histochemistry revealed that the

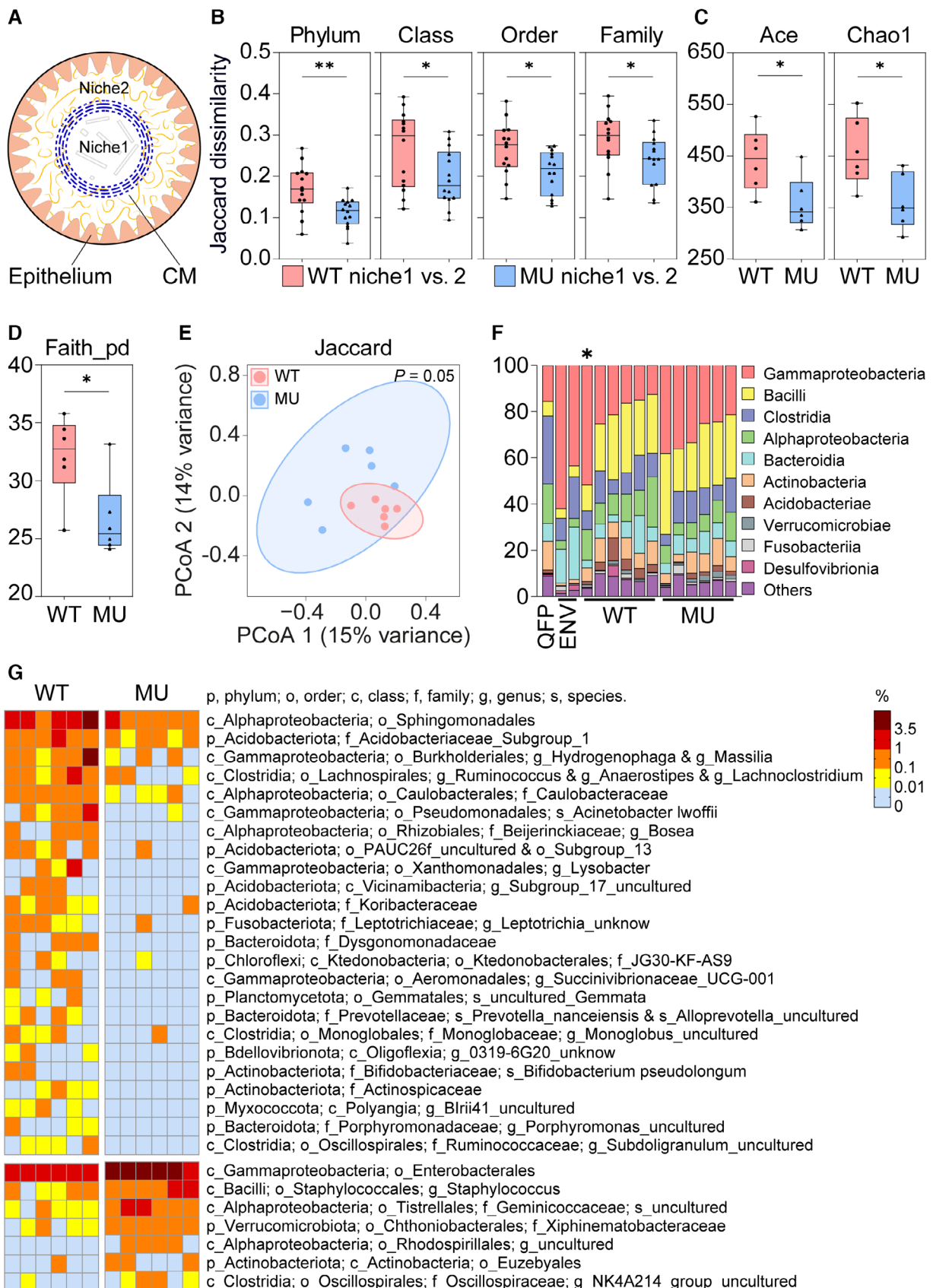


Figure 5.

Figure 5. Role for the CM in maintaining the gut microbiota.

- A Schematic of the radial compartments created by the CM in the gut lumen of zebrafish. The putative niches 1 and 2 for microbiota are indicated.
- B Comparison of 3-month-old wild types and mutants in the pairwise microbiota compositional dissimilarity (Jaccard distance) between the digesta (niche1) and the epithelia (niche2). This metric represents the radial gradient of the gut bacterial composition. The comparison was done on four taxonomy levels. Data of $n = 14$ individuals were represented in box (interquartile range) and whisker (min to max) plots. Individual data points were plotted as black dots. * $P < 0.05$, ** $P < 0.01$ by the conservative, nonparametric Kruskal–Wallis test. Please see Appendix Fig S10 for another way of data presentation, and Dataset EV1 for the details of the sample information and raw statistics. Note that each 16S-rRNA library contains only one sample from one animal.
- C, D Comparison of the bacterial community richness of the intestine samples (S3–S6; including both the digesta and the epithelia) between six 3-month-old wild types and six 3-month-old mutants. Three alpha diversity metrics were used: Ace (abundance-based coverage estimator), Chao1 and Faith_pd (Faith's phylogenetic diversity). Data of $n = 6$ individuals were represented in box (interquartile range) and whisker (min–max) plots. Individual data points were plotted as black dots. * $P < 0.05$ by Kruskal–Wallis test.
- E Principal coordinates analysis (PCoA) of the Jaccard distance (dissimilarity) between samples in (C, D). Data of $n = 6$ individuals were plotted as dots. Ellipses indicated 95% confidence intervals. See Appendix Fig S11 for the PCoA analysis based on the unweighted_unifrac metric.
- F Taxonomic composition measured on the level of class. Asterisk indicated that the genus *Massilia* was abnormally high (~ 28%) in the WT13 sample and removed. QFP, filter paper used to collect microbiota from aquatic environment; ENV, microbiota in aquatic environment. Please see Appendix Fig S12 for the compositional details on other taxonomic levels.
- G Heatmap showing the differentially abundant taxa between the wild-type microbiota and the mutant microbiota (identified by using LEfSe). Each column represented the abundant taxa of gut microbiota of one animal. Please see Appendix Fig S13 for the raw statistic results and Datasets EV2 and EV3 for detailed information of the differentially abundant taxa.

diseased mutant gut was infiltrated with too many cells in the swelling lamina propria and was depleted of mucus (blue colored) in the epithelia (Fig 3I–M). This result was consistent with the high induction of important effectors in the sick mutants (Fig 6D; Datasets EV4 and EV5). Taken together, the results regarding the transcriptomes, anatomy, and histochemistry suggest that young CM-less fish experienced slight gut inflammation, but as their age increased, the inflammation became more serious and could eventually lead to gut atrophy.

CM loss causes no aberrant adaptive responses in young CM-less fish

B/T-cell receptors (BCR/TCR) are hallmark effectors of adaptive immunity. In the fish gut, BCR genes (IgM and IgZ/T) were induced after immune challenges and maintained high expression levels for weeks (Hu *et al*, 2010; Liu *et al*, 2015; Patel *et al*, 2016; Zhang *et al*, 2017; Xu *et al*, 2021). In our rearing conditions, by immersing zebrafish with dead bacteria for 20 min three times in 2 weeks, BCR genes could be induced by tens to hundreds fold for weeks in the gut, gill, and skin. In the 6-month-old sick mutants that suffered from gut atrophy and severe inflammation, the IgM gene was upregulated by at least 25-fold (Fig 6F; Dataset EV4). However, in the gut of 3- and 6-month-old seemingly healthy mutants, we detected no upregulation of BCR and TCR genes (Fig 6F; Dataset EV4). This expression pattern for BCR/TCR was corroborated by the transcriptomes of another eight wild types and eight mutants. Therefore, CM loss did not necessarily cause aberrant adaptive immune responses in young mutants.

Bacterial infection is not responsible for the malnutrition in CM-less fish

In CM-less zebrafish, phenotypes such as malnutrition, slow growth, and gut atrophy could be caused by digestion disorder or microbial infection. To determine the main cause, we cultured and monitored wild-type and mutant fish of the same age in sterile water containing mixed antibiotics. To avoid the long-term toxicity of antibiotics and the development of antibiotic resistance, we used two

sets of antibiotic mixtures and changed them every 2 days. All wild types and mutants survived 5 weeks after the antibiotic treatments, but the mutants still began to show signs of slow growth and gut atrophy (Fig 7G–I; Table EV3). Although we could not rule out viral and parasitic infection, these findings suggest that bacterial and fungal infections were not the main cause of malnutrition in young CM-less zebrafish.

The CM-less gut resists oral gavage of virulent *Vibrio* bacteria

The invertebrate PM is required for gut immunity against microbes (Hegedus *et al*, 2009; Kuraishi *et al*, 2011; Dishaw *et al*, 2016; Rodgers *et al*, 2017). For example, disruption of the PM by nikkomycin Z caused a death rate of 95% in ascidian *Ciona* immersed in pathogenic bacteria (Nakashima *et al*, 2018). However, CM loss did not significantly affect immunity in young fish under our normal rearing conditions. To test whether the gut immunity of CM-less fish could be compromised under more extreme conditions, we administered an extreme dose (20 μ l at 10^{10} CFU/ml) of live virulent *Vibrio* bacterial mixture (*V. anguillarum* and *V. parahaemolyticus*) into the fish gut by oral gavage. To our surprise, neither wild-type nor mutant fish succumbed to this challenge (Fig 7J). This challenge was repeated 3 days later. As a comparison, this dosage is 100 times the lethal dosage (20 μ l at 10^8 CFU/ml), which could kill 100% of wild-type and mutant fish in 1 day if administered through intraperitoneal injection (IP; Fig 7J). Even though the live bacteria were replaced by dead bacteria, this dosage (20 μ l at 10^{10} CFU/ml) killed 90–100% of wild-type and mutant fish in 1 day when administered through IP (Fig 7J).

Discussion

The CM is not a prerequisite for survival, reproduction, and antibacterial immunity

Here, we show that the CM forms into a continuous tube-like structure lining the gut lumen in wild-type zebrafish, regardless of whether there is ingesta in the lumen. Chitin synthase 1 (*chs1*) is

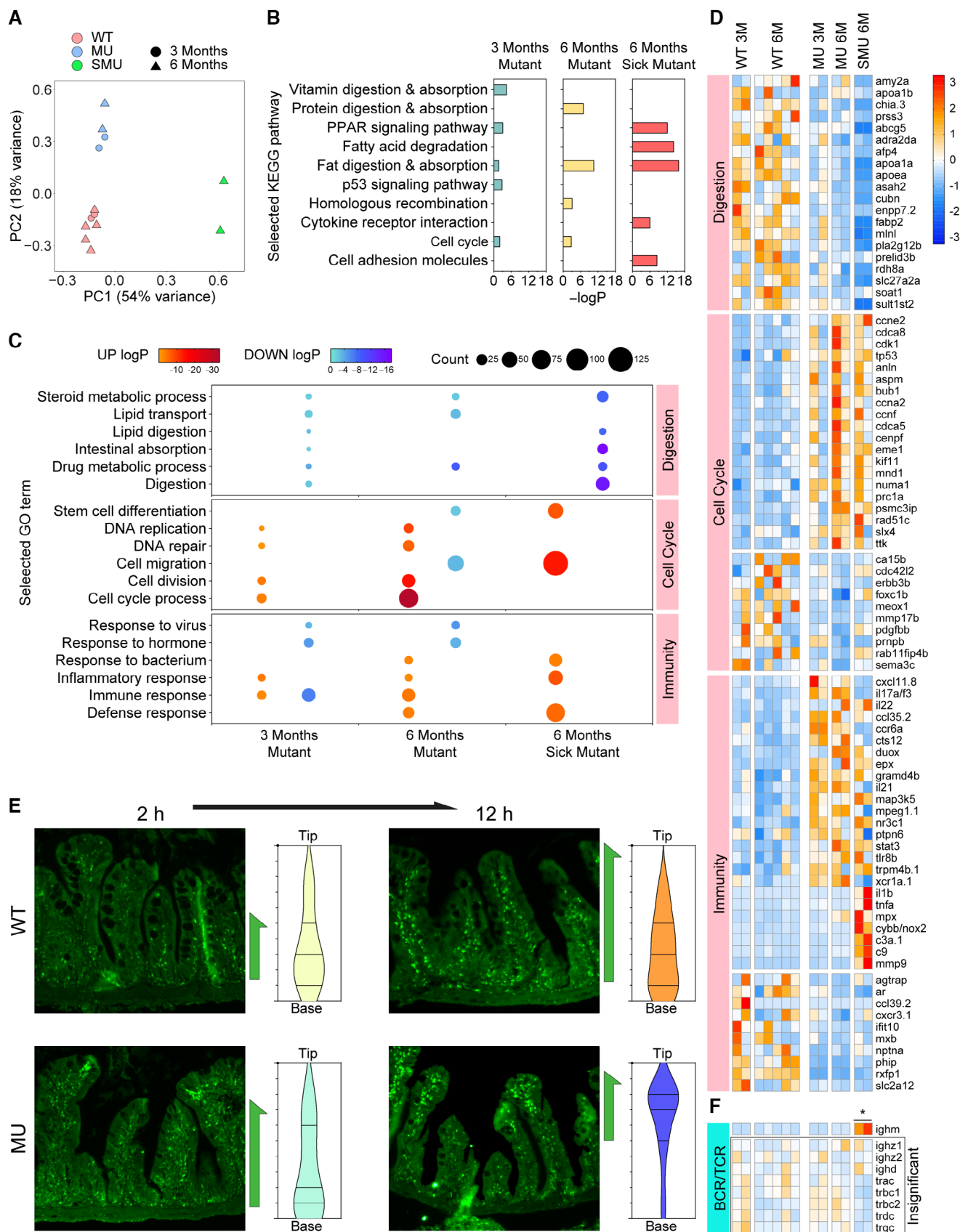


Figure 6.

Figure 6. Effect of CM loss on the gut transcriptomes.

- A Principal component analysis (PCA) of the gut transcriptome (section S3–S6) data showed vast gene expression differences between wild types, seemingly healthy mutants (3- and 6-month-old), and sick mutants (6-month-old). Before analysis, the batch effects in the data were corrected by using Combat (Johnson *et al.*, 2007). Note that each library contains only one tissue sample from one animal. Please see Appendix Fig S14 for more correlation analysis of the transcriptomic profiles.
- B, C Selected KEGG pathways and GO terms of differentially expressed genes (DEGs) in 3-month-old seemingly healthy mutants versus wild types, 6-month-old seemingly healthy mutants versus wild types, and 6-month-old sick mutants versus wild types, respectively. The details of more DEGs analysis were shown in Appendix Figs S15–S19, Datasets EV5 and EV6.
- D Heatmaps showing some prominent DEG genes. Please see Dataset EV4 for a full list of DEG genes and annotations.
- E Immunohistochemical detection of BrdU-labeled cells in the intestine bulb (section S2) of two 3-month-old adult wild types and two 3-month-old adult mutants to measure the rate of cell proliferation (new cells were stained bright green) and migration. Compared with wild types (WT), the mutants had more green spots along the villi 2 h after treatment, and mutants also have more green spots concentrated in the tip of villi 12 h after treatments. The violin plots (interquartile range with mean line) show the relative numbers of green puncta from tip to base of villi, which were calculated from 3 to 5 villi from the raw version of these images. Please see Appendix Fig S19 for the images of more animals and time points.
- F Heatmap showing the expression of BCR and TCR genes, which were not tested significantly between wild types and mutants, except the *ighm* gene that highly increased in the 6-month-old sick mutants.

responsible for CM synthesis and is expressed in most enterocytes throughout the gut. Unlike the invertebrate PM, which is essential for survival and gut immunity (Terra, 2001; Bolognesi *et al.*, 2008; Hegedus *et al.*, 2009; Kuraishi *et al.*, 2011; Dishaw *et al.*, 2016; Rodgers *et al.*, 2017; Nakashima *et al.*, 2018), zebrafish devoid of the CM are viable and fertile and have no external anomalies. Several factors may contribute to the tolerance for CM loss (Fig 8A): (i) young stem cells can maintain gut epithelial integrity by increasing their renewal rates; (ii) few classic PM-binding proteins are disrupted by dislocation due to CM loss; (iii) vertebrate-type mucosal immunity, including adaptive immunity, has the capacity to compensate for the loss of CM-based barrier immunity.

Several findings imply that the capacity of the gut mucosal immunity is intact in young zebrafish: (i) slight inflammation induced by CM loss might help to limit pathogens; (ii) the lack of aberrant adaptive responses in the CM-less gut suggests that adaptive immunity is robust and maintains certain homeostasis; (iii) the administration of antibiotic mixtures failed to alleviate the health issues due to CM loss, suggesting that bacterial infection is not the primary problem in the CM-less gut; (iv) both wild-type and CM-less fish had similar survival rates following an oral gavage of an extreme dose of virulent *Vibrio* bacteria; (v) zebrafish have lost the acidic stomach, which is supposedly required for decimating most of the ingested microbes in other vertebrates (Castro *et al.*, 2014); and (vi) the gel-forming mucin (GFM) MUC2s, which are known to provide important gut barrier immunity against microbes (Johansson *et al.*, 2011; Paone & Cani, 2020), showed no signs of compensation for CM loss. These findings suggest that gut mucosal immunity could compensate for the loss of CM-based barrier immunity in young CM-less fish.

The CM is required for long-term nutrition and health

Although the CM is generally not essential in young zebrafish, it is required for optimal growth, nutrition, and longevity in the long term. Several immediate mechanisms related to the CM-based compartments may potentially contribute to the long-term effects of the fish CM (Fig 8A), which include (i) compacting the ingested substances, (ii) preventing them from jamming the whole gut lumen and invading the epithelia, (iii) facilitating the movement of the gut and digesta, (iv) creating proper niches for the gut microbiota, (v) promoting efficient digestion and absorption, and (vi) relieving gut inflammation and excessive epithelial renewals. Therefore, CM loss

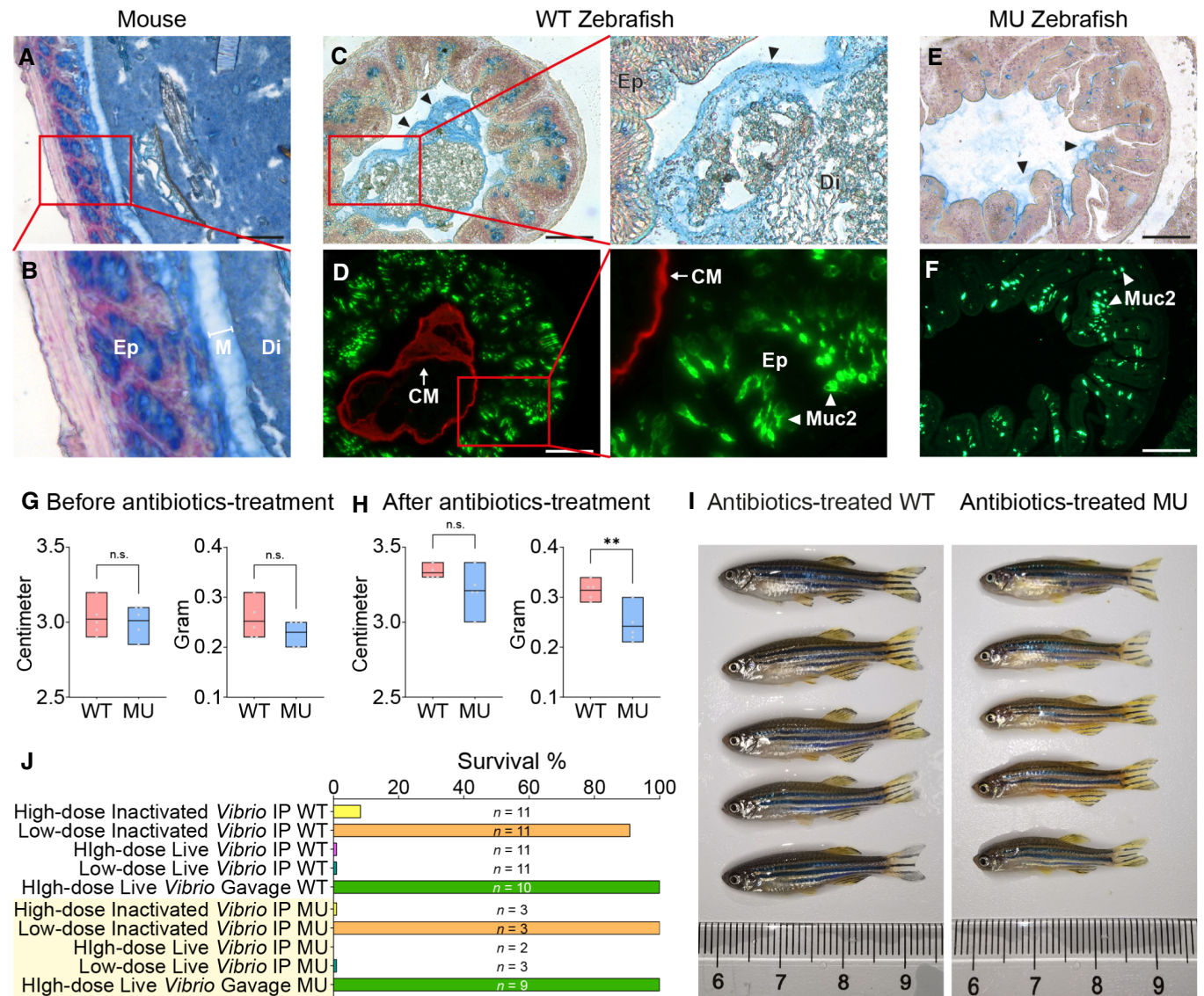
will elicit a series of gut physiology chain reactions, which may be subtle initially but will gradually accumulate to more serious age-dependent health problems, such as malnutrition, slow growth, body emaciation, and gut atrophy, which eventually lead to a small body and a short lifespan.

CM and fish prosperity

The longitudinal gut compartments in fishes are less elaborate than those in mammals (Wang *et al.*, 2010). The acidic stomach was even lost in many fishes, such as zebrafish and tetrodons (Castro *et al.*, 2014; Stumpp *et al.*, 2015). Here, we show that zebrafish could not form firm GFM-based layers to cover the gut epithelia as mammals do. In this sense, preserving the CM may provide certain benefits to fish. A basic difference between CM layers and GFM layers is that chitin can form sturdy and elastic long-chain fibrils. As we showed here, the CM not only prevents the ingesta from touching the epithelia but also compacts the ingesta and squeezes out space between the CM and the gut epithelia, which may permit efficient digestion and quick adaptation to foods with different properties, such as fibrous plants and coarse arthropods, without evolving complex gut structures. Therefore, the CM may contribute to fish prosperity by allowing quick adaptation to a variety of food habits (Nelson *et al.*, 2016; Bar-On *et al.*, 2018; Currie & Evans, 2020). On the contrary, fish gut health and food sources are threatened by pollutants, pathogens, and climate change (Austin, 1998; Portner & Peck, 2010; Fernandes *et al.*, 2013; Townhill *et al.*, 2017; A Maureaud *et al.*, 2021; Kibria *et al.*, 2021; Pepi & Focardi, 2021; Yang *et al.*, 2021). Alternative diets used in cultivated fish also alter their food habits and pose health risks (Green *et al.*, 2013; Wong *et al.*, 2016). In this sense, studying the CM may lead to new strategies to protect fish gut functions, thereby improving fish health and conservation.

Evolution of the radial gut structures in vertebrates

Based on previous findings (Nakashima *et al.*, 2018) and our new findings, we propose two plausible scenarios to explain the evolution of the radial gut structure in vertebrates (Fig 8B). The first scenario is that the CM might be lost by chance (but not necessarily lost completely at the time) because without immediate intolerable phenotypes, a species might evolve compensatory mechanisms if given enough time and conditions. The other scenario concerns tetrapod ancestors leaving



aquatic environments for terrestrial habitats. During the transition, their food sources might become less coarse and less contaminated, and their more selective taste for cleaner and finer foods, possibly together with sharper teeth, might reduce the burden of barrier functions in the gut, eventually allowing the CM to become obsolete.

A CM-less zebrafish model to study gut biology and diseases

Fish are useful models for gut-related diseases (Thomson *et al*, 2012a,b; Kamareddine *et al*, 2020; Ber *et al*, 2021; Lee *et al*, 2021; Montoro-Huguet *et al*, 2021). The discovery of fish CM indicates

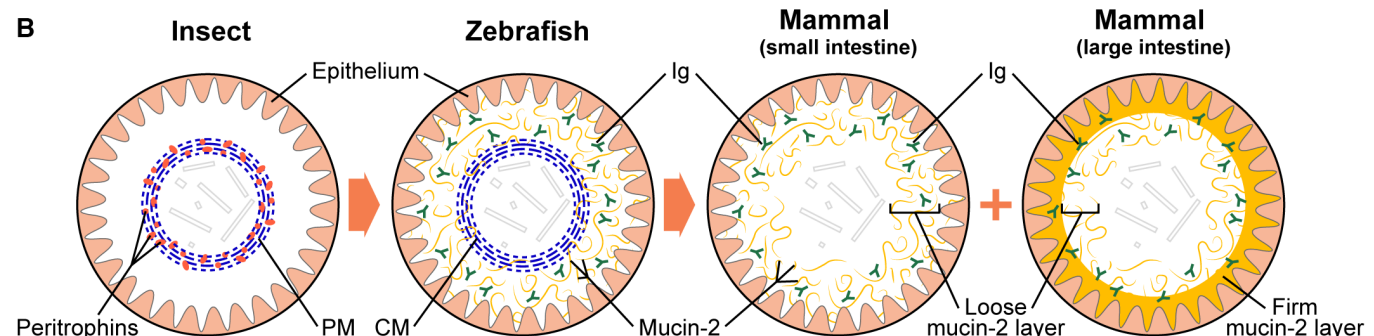
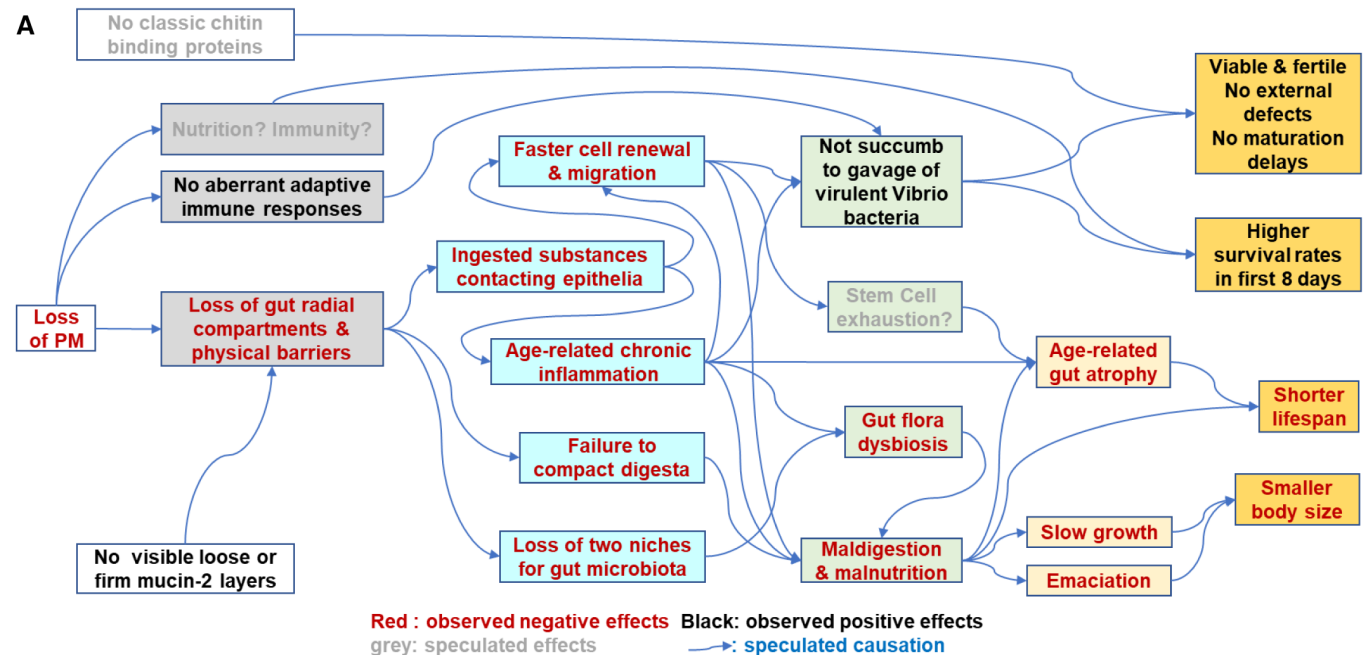


Figure 8. Antibacterial gut immunity in CM-less zebrafish and models for the functional evolution of the gut radial structures.

A Model for the speculated cause-effect relations between different effects observed in the zebrafish with CM loss.
B A proposed model for the evolution of the radial compartments and barriers in the animal intestines.

more differences between fish and mammal gut structures, which affects the comparative studies based on fish models. Nevertheless, the CM-less zebrafish gut has no CM, no firm GFM layers, and no acidic stomach, hence structurally resembling the small intestine of mammals (Fig 8B). In this regard, CM-less zebrafish may be used as a better comparative model for small intestinal diseases.

Materials and Methods

Animals

The AB strain zebrafish were obtained from China Zebrafish Resource Center (CZRC) and maintained in accordance with approved institutional protocols at Sun Yat-Sen University. The rearing and breeding process followed the methods in THE

ZEBRAFISH BOOK (http://zfin.org/zf_info/zfbook/zfbk.html). No special treatments or rearing conditions were used on any zebrafish lines if not specifically described. The CD-1 mice were euthanized with carbon dioxide and donated from Songyang lab at Sun Yat-sen University. All procedures were performed in strict accordance with the recommendations of the Guide for the Care and Use of Laboratory Animals of the National Institutes of Health. The animal use protocol has been reviewed and approved by the Institutional Animal Care and Use Committee (IACUC), Sun Yat-sen University (Approval Number: SYSU-IACUC-2019-B582).

CRISPR-Cas9 mRNA preparation and *chs1* knockout

CRISPRscan (<https://www.crisprscan.org/>) was used to predict potential sgRNA sites on the *chs1* gene locus (Vejnar et al, 2016). The sgRNA DNA templates (Table EV4) were inserted into sgRNA

scaffold of the plasmid 19T-SCFgR by using PCR. PCR products were purified and used to generate sgRNA with AmpliScribe T7-Flash Transcription Kit (Epicenter). The pCS2-nCas9n-*nanos* 3'UTR (62542, Addgene) were linearized and treated by final concentration as 0.2% (v/v) Proteinase K and 0.5% (w/v) SDS at 55°C for 30 min to remove RNase. Clear linearized plasmids were purified and *in vitro* transcribed to Cas9-*nanos* mRNA (SP6 mMessage mMachine Transcription Kit, Ambion). Microinjections containing final concentration as 150 ng/μl sgRNA mRNA and 250 ng/μl Cas9-*nanos* mRNA were carried out at the one-cell stage. Injected embryos were cultivated in E3 buffer at 28°C until feeding.

Genotype confirmation

To determine the genotypes, two–five 3 *dpf* larvae pooled from the same generation or tail-fin tips from individual adults were collected for DNA extraction (Beyotime Biotechnology). The extracted genome DNA was used as PCR templates to amplify the ~500-bp region containing sgRNA site (Table EV4). PCR products were subjected to sequencing and genotyping.

Paraffin sections

Intestines were fixed in methanol-Carnoy's fixative or 4% (w/v) paraformaldehyde (PFA) at 4°C after dissection immediately. Fixed samples were dehydrated in ascending grades of ethanol (70% for 30 min, 90% for 30 min, 95% for 10 min, 100% for 10 min × 2, 100% for 5 min), TO tissue clearing reagent (100% for 5 min × 3) and Paraplast High Melt Wax (Leica) at 65°C (100% for 20 min, 100% for 1 h twice) for embedding. The 6-μm thick sections were prepared by using Leica HistoCore Autocut and stored at room temperature before use. Before staining, all paraffin sections were deparaffinized in descending grades of TO (100% for 5 min), 50% TO and 50% ethanol (3 min), and ethanol (95% for 2 min, 90% for 2 min, 70% for 2 min).

Calcofluor white (CFW) staining

The larvae were incubated to a CFW (diluted as 1:6 in E3 buffer) solution in large plastic Petri dishes for 15 min avoiding light. Larvae were washed and narcotized with 0.5‰ (w/v) MS-222 (MACKLIN) to detect the intake of CFW under the fluorescence microscope. For section staining, deparaffinized sections were incubated with 0.1% (w/v) CFW for 15 min in dark and washed in PBS (10 min × 3).

Purification and conjugation of SNAP-CBD fusion protein

The SNAP-CBD protein from pYZ205 (gifted by Yinhua Zhang, NEB) was expressed as a His-tagged protein and purified by HisTrap FF (GE). The labeling proceeding was according to *Chitin-binding probe with SNAP-CBD fusion* protocol provided by NEB (Maduzia et al, 2011). Briefly, 5 μM SNAP-CBD protein was conjugated with 10 μM SNAP-Surface Alexa Fluor 546 or SNAP-Surface 594 substrate in PBS with 1 mM DTT for 1 h at 37°C. Labeled protein was dialyzed in PBS with 1 mM DTT overnight and stored in –20°C. Prethawed at 4°C before using.

SNAP-CBD staining

Whole-mount staining of PFA-fixed larvae was processed according to the modified protocol (Tang et al, 2015). Briefly, fixed larvae were treated with 1% (v/v) Triton X-100 overnight to improve permeability additionally, blocked in 5% (w/v) Bovine Serum Albumin (BSA), and incubated with SNAP-CBD fluorescent protein over 12 h at 4°C. Intestinal sections were deparaffinized and placed in 10 mM sodium citrate buffer (1.8 mM C₆H₈O₇.H₂O, 8.2 mM Na₃C₆H₅O₇.2 H₂O, pH 6.0) for 20 min at 98°C for antigen retrieval (Abd-Elhafeez et al, 2020). Sections were blocked and assayed for chitin in the same manner as larvae.

Chitinase digestion assay

Deparaffinized sections were treated with 0.1% (w/v) chitinase solution (pH 6.0, Chitinase from *Streptomyces griseus*; Sigma) or PBS at 37°C overnight and washed (Dishaw et al, 2016). Treated sections were immunodetected by SNAP-CBD fluorescent protein.

Alcian blue staining

To stain the intestinal mucus in zebrafish and mice, the Alcian blue method (pH 2.5, Mucin Stain; Abcam) was used. Deparaffinized sections were pretreated with acetic acid solution and washed in distilled H₂O (2 min). Alcian blue solution was applied for 30 min and then rinsed. Sections were incubated in nuclear fast red solution for 5 min and followed by a quick wash in distilled H₂O.

Anti-drMuc2.1/2.4 staining

A polyclonal serum/antibody was raised against a shared epitope of zebrafish Muc2.1/Muc2.4 (TTTTTPVPPPTTTPVPTTTT in the PTS region) and tested. Deparaffinized sections were retrieved by sodium citrate buffer, blocked in 5% BSA, incubated with a polyclonal serum against the zebrafish Muc2.1/Muc2.4 at 4°C overnight, and then rinsed in PBS thoroughly. Anti-rabbit antibody labeled with Alexa Fluor 488 (CST, 4412S) was applied for 2 h and followed with three washes in PBS (5 min). After 5 min incubation with DAPI, these sections were washed in PBS (5 min × 3) and mounted.

Survival rates and body size measurement

Larvae were cultivated in E3 buffer, and the survival rates were recorded every day. The survival rates of adults were recorded every 2 weeks. A special 90-day monitoring program was also carried out and the records were taken at 0 *dpf*, 7 *dpf*, 30 *dpf*, and 90 *dpf*. At 3- and 6-month-old, adults were anesthetized briefly with 0.5‰ (w/v) MS-222 and then subjected to the measurement of body length and weight.

The 16S rRNA gene amplicon analysis

All wild-type animals used in these experiments were the same population from the same group of parents, and so did all mutants. All animals were reared in the same small aquarium system with 300–500 l of water, but distributed in different boxes. Feeding and starving were also done in this system. However, they were collected

and sequenced in different batches. Adult zebrafish (3–3.5 months old) were euthanized with MS-222, and the surface was carefully wiped with 75% ethanol for sterilization. The intestine was isolated by dissection and preserved in sterile PBS on ice. To compare the digested content and the epithelium tissues, the digested content was isolated from the intestine and preserved in sterile PBS, whereas the remaining intestine tissue was washed briefly in sterile PBS on ice. Specifically, under microscopy, the whole digested content (with CM) could be carefully pulled out after slitting open the gut longitudinally (Appendix Fig S9). After dissection, all tissues were frozen in liquid nitrogen for 5 min and stored at –80°C. The composition of gut bacteria in each sample was analyzed using sequencing of 16S rRNA gene amplicons. DNA was extracted from each sample using CTAB methods. The V3–V4 variable regions of the 16S rRNA genes were amplified with the primer pair 338F (5'-ACTCCTACGGAGGCAGCA-3') and 806R (5'-GGACTACHVGGGTW TCTAAT-3'). Each library contains only one tissue sample from one animal. After the libraries were built, the PE250 sequencing was performed using the Illumina NovaSeq 6000 platform. Raw reads were available under BioProject accession number [PRJNA798186] and [PRJNA798182].

Raw reads were filtered by using Trimmomatic v.0.33 with default parameters (Bolger *et al*, 2014). Adapters were trimmed to generate clean reads by using cutadapt 1.9.1 (Martin, 2011). Forward reads and reverse reads were first merged by using the fastq_mergepairs command of USEARCH v.11 and then subjected to further quality filtering using the fastq_filter command of USEARCH v.11 (with fastq_maxee set to 2.0; Edgar, 2010). Filtered reads from different samples were pooled together to detect unique sequences as suggested by the USEARCH manual. Each sample was then denoised, chimera-filtered, and dereplicated against unique sequence independently using the Unoise3 plugin of USEARCH v.11 (default parameter; preprint: Edgar, 2016). The obtained reads with 100% nucleotide sequence identity were considered zero operational taxonomic units (ZOTUs). For comparison, we also ran Uparse with default parameter (Edgar, 2013), to generate operational taxonomic units (OTUs) which were preclustered at 97% sequence identity. For downstream analysis, both ZOTU and OTU datasets were imported as feature tables into the QIIME2 pipeline (v.2021.8; Bolyen *et al*, 2019).

Taxonomy was assigned to ZOTUs and OTUs using a newly trained sk-learn naive Bayes classifier in the feature-classifier plugin of QIIME2 (Bokulich *et al*, 2018). This naive Bayes classifier was trained using Silva reference database (Release 138.1; <https://www.arb-silva.de/>) and the primer pair (338F/806R) for the V3–V4 region of the 16S rRNA genes. If not specified, ZOTU and OTU features were filtered out if they had less than eight reads or presented in less than two samples before downstream analyses. Phylogenetic trees were built for ZOTUs and OTUs by using the phylogeny plugin of QIIME2. The FastTree algorithm was used for this purpose (Price *et al*, 2010). Alpha diversity and beta diversity were calculated using rarefied samples by core metrics suggested by QIIME2. Results of alpha and beta diversity are further processed and visualized using R v.4.1.2 (<https://www.r-project.org/>; R Core Team, 2019). Differentially abundant taxa (or marker taxa) between groups were identified by using the linear discriminant analysis effect size (LEfSe) analysis (Segata *et al*, 2011), which is supposed to provide a more conservative estimate than other methods.

RNA extraction and cDNA synthesis

Total RNA was extracted from different developmental stages and adult tissues. Ten to twenty embryos or larvae at each developmental stage were collected and pooled together. Gill, heart, intestine, spleen, liver, kidney, skin, and muscle were harvested from four adult fish. Ovary and testis were collected from two females and males, respectively. The intestinal tissues harvested from four adult fish were subdivided into esophagus, S1, S2, S3, S4, S5, S6, and S7 regions. Total RNA was extracted and purified by using the TRIzol reagent and the TRIzol Plus RNA Purification Kit. Purified RNA was examined by agarose gel electrophoresis and quantified using NanoDrop. RNA was reverse-transcribed into cDNA (PrimeScript II 1st Strand cDNA Synthesis Kit, TaKaRa).

Quantitative real-time RT-PCR

Primers for quantitative real-time RT-PCR (qRT-PCR) were designed using Beacon Designer (Table EV4). The qRT-PCR was performed in 10 µl volume with SYBR Green Realtime PCR Master Mix (TOYOBO) according to the manufacturer's instructions. Samples were run in triplet following this PCR procedure: predenaturation (30 s at 95°C), amplification (5 s at 92°C, 10 s at 58–60°C, and 20 s at 72°C), final extension (1 s at 75°C), and curving (5/30 s at 95/60°C). First-strand cDNA was diluted in a series of gradient to establish the calibration curves. The slope of the calibration was converted into efficiency (%) by log-linear formula as suggested (Bustin *et al*, 2009). Data were quantified with $2^{-\Delta\Delta C_t}$ method based on C_t values of *chs1*, *chs2*, *chs4*, and *actb2* (Casadei *et al*, 2011). For the expression during embryogenesis, folds were normalized to the *chs2* expression level at 24 hpf. For the expression in adult tissues, folds were normalized to the *chs4* expression level in muscle. For the expression in different gut sections, folds were normalized to the *chs1* expression level in the esophagus. The expression levels of *mucin* genes were quantified with the $2^{-\Delta\Delta C_t}$ method based on C_t values of *actb1*.

RNA-seq

Total RNA of the gut samples from single fishes was extracted by using RNeasy Plus Mini Kit (Qiagen) following the manufacturer's protocol. Each library contains only one tissue for one animal. The RNA concentration was measured using NanoDrop, and the RNA integrity was determined using Qseq1 (Bioptic). Total RNA was enriched by Oligo(dT)-attached magnetic beads and then randomly fragmented in fragmentation buffer. Random-hexamer primers were used to synthesize first-strand cDNA, and RNase H, DNA polymerase I, dNTPs were added subsequently for second-strand cDNA synthesis. Double-strand cDNA fragments were end-repaired, ligated with adapters, and selectively purified by AMPure XP (Beckman coulter) to generate libraries. Libraries were sequenced on the Illumina NovaSeq 6000 platform to generate 150-bp paired-end reads. The RNA-seq data are available under the BioProject accession number [PRJNA781427].

Bulk transcriptome analysis

Reference genome (assembly GRCz11; GCF_000002035.6) and gene model annotation files of *Danio rerio* were downloaded from the

NCBI genome website. Human-zebrafish gene orthologs (ZFIN: http://zfin.org/downloads/human_orthos.txt) and gene homolog were used to further annotate the zebrafish gene functions. Several genes that do not have correct gene models, such as B-cell receptor genes (IgM, IgD, IgZ1, and IgZ2), T-cell receptor genes, and mucin genes, were manually created and annotated. Raw RNA-seq data were cleaned using Trimmomatic v.0.36 with default parameters for quality control (Bolger *et al.*, 2014). The clean data were mapped to the zebrafish reference genome using Hisat2 v.2.1.0 under default parameters (Pertea *et al.*, 2016). StringTie v.2.0.4 was used to assemble transcripts and quantify gene abundance. The fragments per kilobase of exon model per million mapped fragments (FPKM) of each gene were calculated. When the data free of batch effects were required, the ComBat nonparametric method was used to correct the FPKM values (Johnson *et al.*, 2007). Sample principal component analysis (PCA) based on the corrected FPKM values was performed using the “prcomp” function in R (<http://www.r-project.org>). Differentially expressed genes (DEG) were identified using DESeq2 as genes having $|\log_2 \text{fold change}| > 1.5$ and $P\text{-values} < 0.05$ (Love *et al.*, 2014). Gene ontology (GO) and Kyoto encyclopedia of genes and genomes (KEGG) analysis of zebrafish DEGs were performed using Metascape (<https://metascape.org/>; Zhou *et al.*, 2019). GO and KEGG terms with $P\text{-values} < 0.01$ were considered significantly enriched.

Single-cell transcriptome analysis

Reference genome (assembly GRCz11) and gene model annotation files (Ensembl release 98) of *Danio rerio* were downloaded from the Ensembl genome website. Adult zebrafish (AB strain) gut scRNA-seq datasets were obtained from the Gene Expression Omnibus (GEO) database [accession: GSE136109] (Data ref: Gu *et al.*, 2019; Gu *et al.*, 2020). Sequenced reads were mapped to the zebrafish reference genome, and the gene quantification was performed using Cell Ranger software v.4.0.0. The cell clustering was based on the K -means clustering algorithm ($K = 7$). The DEGs of specific cell clusters were identified using Loupe Cell Browser v.5.0.0, the visualization software provided by 10X Genomics.

Bromodeoxyuridine (BrdU) assays

The assays were conducted as described previously (Wallace *et al.*, 2005). Briefly, a volume of 20 μl 15 mM BrdU (Sigma) was intraperitoneally injected into 3-month-old zebrafish. 2 and 12 h after injection, intestines were isolated from the euthanized zebrafish, fixed in 4% PFA at 4°C, and cut in 6- μm sections. To denature DNA, deparaffinized sections were incubated in 2 M HCl for 30 min at 37°C. After blocking with 5% (w/v) BSA with 0.01% (v/v) Triton X-100, the sections were incubated with the mouse Anti-BrdU antibody (Abcam, ab8152) in the immunohistochemical wet box at 4°C overnight, and the anti-mouse Alexa Fluor 488 (Thermo Fisher Scientific, A11029) was used as the secondary antibody for 2 h.

Long-term antibiotics treatments

Eight-week-old fish of similar body sizes were collected for the experiment. The fish were cultured in sterile water with the supplement of two different sets of antibiotics mixtures (set A: 20 mg/l

ampicillin, 20 mg/l kanamycin, 200 mg/l metronidazole, 50 mg/l oxytetracycline; set B: 2 mg/l furazolidone, 50 mg/l azithromycin, 20 mg/l fungicide amphotericin B, 10 mg/l vancomycin), which were changed every 2 days. The fish were observed for 6 weeks. The body length and weight were recorded in the fifth week.

Intraperitoneal injection and gavage

The 4–5 month-old zebrafish were used in this experiment. The soft sponge with a notch was prepared and soaked in 0.5% (w/v) MS-222. Fishes were anesthetized and positioned with the abdomen up in notch on the sponge. For intraperitoneal injection, the insulin syringe needle (Needle gauge O.D. 0.33 mm \times Length 13 mm) was inserted carefully into the midline between the pelvic fins (Kinkel *et al.*, 2010). For gavage, the insulin syringe was attached to a 1.2 cm polyethylene microcatheter (I.D. 0.38 mm \times O.D. 1.09 mm; Collymore *et al.*, 2013). The microcatheter was used to open the mouth and inserted down to the esophagus, avoiding the gill and heart. The gavage was applied slowly to avoid the solution from flowing out of the gills and mouth. After injection or gavage, fishes were transferred to clean water immediately for recovery. Once they had recovered, they were returned to tanks and raised as usual.

Vibrio bacterial challenge

Zebrafish is a proposed model for studying pathogenic *Vibrios* (Nag *et al.*, 2020) and has been shown to require the adaptive immunity to control *Vibrios* in the gut (Brugman *et al.*, 2014). Virulent strains of *Vibrio parahaemolyticus* (Peng *et al.*, 2016) and *Vibrio anguillarum* (from Marine Culture Collection of China), which are fish pathogen bacteria, were grown in seawater medium (0.1% yeast extract, 0.5% tryptone, 3.3% sodium chloride) and LB20 medium (0.5% yeast extract, 1% tryptone, 2% sodium chloride) at 30°C for 16 h, respectively. Inactivated bacteria were produced by incubation with a final concentration of 0.4% formalin over 24 h and collected by centrifuge at 6,000 g for 5 min at 4°C after thrice thorough washes in sterile PBS. Live bacteria were centrifuged at 6,000 g for 5 min at 4°C and washed in sterile PBS twice. An equal volume of two *Vibrio* species were mixed before use and diluted to the desired concentration (10^{10} CFU/ml or 10^8 CFU/ml) in sterile PBS. Six different treatments for adult zebrafish were conducted: (i) low-dose intraperitoneal injection (IP) of wild-type fishes with killed *Vibrio*, (ii) low-dose IP of wild types with live *Vibrio*, (iii) high-dose IP of wild types with killed *Vibrio*, (iv) high-dose IP of wild types with live *Vibrio*, (v) high-dose gavage of wild types with live *Vibrio*, (vi) high-dose gavage of mutants with live *Vibrio*. Each fish was administrated with 20 μl bacterial mixture. After treatment, the survival rates were monitored for 10 days.

Microscopy

Microscope optical images were created using Leica DMi8 inverted fluorescence microscope equipped with microsystems CMS GmbH. Confocal images were taken with Leica TCS SP8.

Live imaging of the larvae gut

The 6–7 dpf larvae were fed with 6 μm dyed polystyrene beads (Polybead microsphere) for 12–24 h. Larvae were anesthetized with

0.2–0.4% (w/v) MS-222 and placed on glass slides with E3 buffer or 3% methylcellulose. Pictures were taken every 3–5 s with a Leica DMI8 microscope. Pictures were stitched into motion pictures by using Adobe Premiere.

Statistical analysis

The data collected from the qRT-PCR and body size measurement were analyzed using two-tailed *t*-test with unequal variation by using Excel 2016 and GraphPad Prism v.9.0.0 or one-way multivariate analysis of variance (MANOVA) test using dplyr R package. *P*-values of the survival analysis were determined by log-rank (Mantel-Cox) test. The plots of beta diversity were produced by principal coordinates analysis (PCoA) calculated by using QIIME2 core metrics to indicate dissimilarities between samples. The ellipse with a 95% confidence level for a multivariate *t*-distribution was added to scatter plots by using ggplot2 R package. Nonparametric variables in the microbiota analysis, including the alpha diversity metrics and the pairwise dissimilarities between gut epithelium and gut content, were tested using the Kruskal-Wallis test. *P*-values < 0.05, < 0.01, and < 0.001 were regarded as significant, very significant, and extremely significant, respectively.

Data availability

The raw data of bulk RNA-seq were submitted under NCBI BioProject accession PRJNA781427 (<https://www.ncbi.nlm.nih.gov/bioproject/?term=PRJNA781427>). The raw reads of 16S rDNA-seq were submitted under NCBI BioProject accession PRJNA798186 (<https://www.ncbi.nlm.nih.gov/bioproject/?term=PRJNA798186>) and PRJNA798182 (<https://www.ncbi.nlm.nih.gov/bioproject/?term=PRJNA798182>).

Expanded View for this article is available [online](#).

Acknowledgements

We thank Dr. Yinhua Zhang of NEB for providing pYZ205. Mouse sample was obtained from the Lab of Professor Zhou Songyang. This work was supported by National Key R&D program of China (2018YFD0900503), NNSF Project (31971107 & 31722052), projects of Southern Marine Science and Engineering Guangdong Laboratory (Zhuhai; SML2021SP304 & 311021006), projects from Guangdong and Guangzhou (2021A1515012380 & 2020B1212060031), Fundamental Research Funds for the Central Universities (Sun Yat-sen University; 22lgj09), decoding TCM project of BUCM (90010060920009), National Key R&D Project (2019YFC1710104) and NNSF Project (91942301).

Author contributions

Zirui Yue: Conceptualization; resources; data curation; formal analysis; validation; investigation; visualization; writing – original draft. **Zhaoyu Fan:** Resources; data curation; validation; investigation; visualization. **Hao Zhang:** Resources; data curation; software; validation; investigation; visualization; methodology. **Buhan Feng:** Resources; data curation; software; formal analysis; validation; investigation; visualization; methodology. **Chengyi Wu:** Resources; data curation; formal analysis; investigation; methodology. **Shenghui Chen:** Resources; project administration. **Jihua Ouyang:** Visualization; methodology. **Huiping Fan:** Resources; investigation. **Panwei Weng:** Resources; investigation. **Huixiong Feng:** Resources. **Shangwu Chen:**

Supervision; funding acquisition; project administration. **Meiling Dong:** Supervision; funding acquisition; project administration. **Anlong Xu:** Resources; supervision; funding acquisition; project administration; writing – review and editing. **Shengfeng Huang:** Conceptualization; resources; data curation; formal analysis; supervision; funding acquisition; methodology; writing – original draft; project administration; writing – review and editing.

Disclosure and competing interests statement

The authors declare that they have no conflict of interest.

References

- A Maureaud A, Frelat R, Pecuchet L, Shackell N, Merigot B, Pinsky ML, Amador K, Anderson SC, Arkhipkin A, Auber A et al (2021) Are we ready to track climate-driven shifts in marine species across international boundaries? A global survey of scientific bottom trawl data. *Glob Chang Biol* 27: 220–236
- Abd-Elhafeez HH, Abou-Elhamd AS, Soliman SA (2020) Morphological and immunohistochemical phenotype of TCs in the intestinal bulb of grass carp and their potential role in intestinal immunity. *Sci Rep* 10: 14039
- Agace WW, McCoy KD (2017) Regionalized development and maintenance of the intestinal adaptive immune landscape. *Immunity* 46: 532–548
- Austin B (1998) The effects of pollution on fish health. *J Appl Microbiol* 85: 234S–242S
- Bar-On YM, Phillips R, Milo R (2018) The biomass distribution on earth. *Proc Natl Acad Sci U S A* 115: 6506–6511
- Ber Y, García-López S, Gargallo-Puyuelo CJ, Gomollón F (2021) Small and large intestine (II): inflammatory bowel disease, short bowel syndrome, and malignant tumors of the digestive tract. *Nutrients* 13: 2325
- Bokulich NA, Kaehler BD, Rideout JR, Dillon M, Bolyen E, Knight R, Huttley GA, Gregory Caporaso J (2018) Optimizing taxonomic classification of marker-gene amplicon sequences with QIIME 2's q2-feature-classifier plugin. *Microbiome* 6: 90
- Bolger AM, Lohse M, Usadel B (2014) Trimmomatic: a flexible trimmer for Illumina sequence data. *Bioinformatics* 30: 2114–2120
- Bolognesi R, Terra WR, Ferreira C (2008) Peritrophic membrane role in enhancing digestive efficiency. Theoretical and experimental models. *J Insect Physiol* 54: 1413–1422
- Bolyen E, Rideout JR, Dillon MR, Bokulich NA, Abnet CC, Al-Ghalith GA, Alexander H, Alm Ej, Arumugam M, Asnicar F et al (2019) Reproducible, interactive, scalable and extensible microbiome data science using QIIME 2. *Nat Biotechnol* 37: 852–857
- Brown H, Esterhazy D (2021) Intestinal immune compartmentalization: implications of tissue specific determinants in health and disease. *Mucosal Immunol* 14: 1259–1270
- Brugman S, Schneeberger K, Witte M, Klein MR, van den Bogert B, Boekhorst J, Timmerman HM, Boes ML, Kleerebezem M, Nieuwenhuis EE (2014) T lymphocytes control microbial composition by regulating the abundance of vibrio in the zebrafish gut. *Gut Microbes* 5: 737–747
- Bunker JJ, Bendelac A (2018) IgA responses to microbiota. *Immunity* 49: 211–224
- Bustin SA, Benes V, Garson JA, Hellemans J, Huggett J, Kubista M, Mueller R, Nolan T, Pfaffl MW, Shipley GL et al (2009) The MIQE guidelines: minimum information for publication of quantitative real-time PCR experiments. *Clin Chem* 55: 611–622
- Casadei R, Pelleri MC, Vitale L, Facchini F, Lenzi L, Canaider S, Strippoli P, Frabetti F (2011) Identification of housekeeping genes suitable for gene expression analysis in the zebrafish. *Gene Expr Patterns* 11: 271–276

- Castro LF, Goncalves O, Mazan S, Tay BH, Venkatesh B, Wilson JM (2014) Recurrent gene loss correlates with the evolution of stomach phenotypes in gnathostome history. *Proc Biol Sci* 281: 20132669
- Cazares-Raga FE, Chavez-Munguia B, Gonzalez-Calixto C, Ochoa-Franco AP, Gwinowicz MA, Rodriguez MH, Hernandez-Hernandez FC (2014) Morphological and proteomic characterization of midgut of the malaria vector *Anopheles albimanus* at early time after a blood feeding. *J Proteomics* 111: 100–112
- Collymore C, Rasmussen S, Tolwani RJ (2013) Gavaging adult zebrafish. *J Vis Exp* 78: 50691
- Colston TJ, Jackson CR (2016) Microbiome evolution along divergent branches of the vertebrate tree of life: what is known and unknown. *Mol Ecol* 25: 3776–3800
- Currie S, Evans DH (2020) *The physiology of fishes*. Boca Raton, FL: CRC Press
- Dishaw LJ, Leigh B, Cannon JP, Liberti A, Mueller MG, Skapura DP, Karrer CR, Pinto MR, De Santis R, Litman GW (2016) Gut immunity in a protostome involves a secreted immunoglobulin-type mediator binding host chitin and bacteria. *Nat Commun* 7: 10617
- Edgar RC (2010) Search and clustering orders of magnitude faster than BLAST. *Bioinformatics* 26: 2460–2461
- Edgar RC (2013) UPARSE: highly accurate OTU sequences from microbial amplicon reads. *Nat Methods* 10: 996–998
- Edgar RC (2016) UNOISE2: improved error-correction for Illumina 16S and ITS amplicon sequencing. *bioRxiv* <https://doi.org/10.1101/081257> [PREPRINT]
- Edwards MJ, Jacobs-Lorena M (2000) Permeability and disruption of the peritrophic matrix and caecal membrane from *Aedes aegypti* and *Anopheles gambiae* mosquito larvae. *J Insect Physiol* 46: 1313–1320
- Fernandes JA, Cheung WW, Jennings S, Butenschon M, de Mora L, Frolicher TL, Barange M, Grant A (2013) Modelling the effects of climate change on the distribution and production of marine fishes: accounting for trophic interactions in a dynamic bioclimate envelope model. *Glob Chang Biol* 19: 2596–2607
- Flores MV, Crawford KC, Pullin LM, Hall CJ, Crosier KE, Crosier PS (2010) Dual oxidase in the intestinal epithelium of zebrafish larvae has anti-bacterial properties. *Biochem Biophys Res Commun* 400: 164–168
- Gomez D, Sunyer JO, Salinas I (2013) The mucosal immune system of fish: the evolution of tolerating commensals while fighting pathogens. *Fish Shellfish Immunol* 35: 1729–1739
- Grasberger H, Gao J, Nagao-Kitamoto H, Kitamoto S, Zhang M, Kamada N, Eaton KA, El-Zaatari M, Shreiner AB, Merchant JL et al (2015) Increased expression of DUOX2 is an epithelial response to mucosal dysbiosis required for immune homeostasis in mouse intestine. *Gastroenterology* 149: 1849–1859
- Green TJ, Smullen R, Barnes AC (2013) Dietary soybean protein concentrate-induced intestinal disorder in marine farmed Atlantic salmon, *Salmo salar* is associated with alterations in gut microbiota. *Vet Microbiol* 166: 286–292
- Gu W, Liu S, Chen L, Liu Y, Gu C, Ren H-q, Wu B (2019) Gene Expression Omnibus GSE136109 (<https://www.ncbi.nlm.nih.gov/geo/query/acc.cgi?acc=GSE136109>). [DATASET]
- Gu W, Liu S, Chen L, Liu Y, Gu C, Ren HQ, Wu B (2020) Single-cell RNA sequencing reveals size-dependent effects of polystyrene microplastics on immune and secretory cell populations from zebrafish intestines. *Environ Sci Technol* 54: 3417–3427
- Hegedus D, Erlandson M, Gillott C, Toprak U (2009) New insights into peritrophic matrix synthesis, architecture, and function. *Annu Rev Entomol* 54: 285–302
- Hu YL, Xiang LX, Shao JZ (2010) Identification and characterization of a novel immunoglobulin Z isotype in zebrafish: implications for a distinct B cell receptor in lower vertebrates. *Mol Immunol* 47: 738–746
- Jevtov I, Samuelsson T, Yao G, Amsterdam A, Ribbeck K (2014) Zebrafish as a model to study live mucus physiology. *Sci Rep* 4: 6653
- Johansson ME, Larsson JM, Hansson GC (2011) The two mucus layers of colon are organized by the MUC2 mucin, whereas the outer layer is a legislator of host-microbial interactions. *Proc Natl Acad Sci U S A* 108: 4659–4665
- Johansson ME, Sjovall H, Hansson GC (2013) The gastrointestinal mucus system in health and disease. *Nat Rev Gastroenterol Hepatol* 10: 352–361
- Johansson ME, Gustafsson JK, Holmen-Larsson J, Jabbar KS, Xia L, Xu H, Ghishan FK, Carvalho FA, Gewirtz AT, Sjovall H et al (2014) Bacteria penetrate the normally impenetrable inner colon mucus layer in both murine colitis models and patients with ulcerative colitis. *Gut* 63: 281–291
- Johnson WE, Li C, Rabinovic A (2007) Adjusting batch effects in microarray expression data using empirical Bayes methods. *Biostatistics* 8: 118–127
- Kamareddine L, Najjar H, Sohail MU, Abdulkader H, Al-Asmakh M (2020) The microbiota and gut-related disorders: insights from animal models. *Cell* 9: 2401
- Kelkenberg M, Odman-Naresh J, Muthukrishnan S, Merzendorfer H (2015) Chitin is a necessary component to maintain the barrier function of the peritrophic matrix in the insect midgut. *Insect Biochem Mol Biol* 56: 21–28
- Kibria G, Nuggeoda D, Rose G, Haroon AKY (2021) Climate change impacts on pollutants mobilization and interactive effects of climate change and pollutants on toxicity and bioaccumulation of pollutants in estuarine and marine biota and linkage to seafood security. *Mar Pollut Bull* 167: 112364
- Kinkel MD, Eames SC, Philipson LH, Prince VE (2010) Intraperitoneal injection into adult zebrafish. *J Vis Exp* 42: 2126
- Kuraishi T, Binggeli O, Opota O, Buchon N, Lemaitre B (2011) Genetic evidence for a protective role of the peritrophic matrix against intestinal bacterial infection in *Drosophila melanogaster*. *Proc Natl Acad Sci U S A* 108: 15966–15971
- Lee JG, Cho HJ, Jeong YM, Lee JS (2021) Genetic approaches using zebrafish to study the microbiota-gut-brain axis in neurological disorders. *Cell* 10: 566
- Lescak EA, Milligan-Myhre KC (2017) Teleosts as model organisms to understand host-microbe interactions. *J Bacteriol* 199: e00868-16
- Liu X, Wu H, Liu Q, Wang Q, Xiao J, Chang X, Zhang Y (2015) Profiling immune response in zebrafish intestine, skin, spleen and kidney bath-vaccinated with a live attenuated vibrio anguillarum vaccine. *Fish Shellfish Immunol* 45: 342–345
- Love MI, Huber W, Anders S (2014) Moderated estimation of fold change and dispersion for RNA-seq data with DESeq2. *Genome Biol* 15: 550
- Maduzia LL, Yu E, Zhang Y (2011) *Caenorhabditis elegans* galectins LEC-6 and LEC-10 interact with similar glycoconjugates in the intestine. *J Biol Chem* 286: 4371–4381
- Martin M (2011) Cutadapt removes adapter sequences from high-throughput sequencing reads. *EMBnet* 17 <https://doi.org/10.14806/ej.17.1.200>
- Martinsen TC, Bergh K, Waldum HL (2005) Gastric juice: a barrier against infectious diseases. *Basic Clin Pharmacol Toxicol* 96: 94–102
- Merzendorfer H (2011) The cellular basis of chitin synthesis in fungi and insects: common principles and differences. *Eur J Cell Biol* 90: 759–769
- Montoro-Huguet MA, Belloc B, Dominguez-Cajal M (2021) Small and large intestine (I): malabsorption of nutrients. *Nutrients* 13: 1254
- Mowat AM, Agace WW (2014) Regional specialization within the intestinal immune system. *Nat Rev Immunol* 14: 667–685
- Nag D, Farr DA, Walton MG, Withey JH (2020) Zebrafish models for pathogenic Vibrios. *J Bacteriol* 202: e00165-20
- Nakashima K, Kimura S, Ogawa Y, Watanabe S, Soma S, Kaneko T, Yamada L, Sawada H, Tung CH, Lu TM et al (2018) Chitin-based barrier immunity

- and its loss predated mucus-colonization by indigenous gut microbiota. *Nat Commun* 9: 3402
- Nelson JS, Grande TC, Wilson MVH (2016) *Fishes of the world*. Hoboken, NJ: Wiley Press
- Niethammer P, Grabher C, Look AT, Mitchison TJ (2009) A tissue-scale gradient of hydrogen peroxide mediates rapid wound detection in zebrafish. *Nature* 459: 996–999
- Pais IS, Valente RS, Sporniak M, Teixeira L (2018) Drosophila melanogaster establishes a species-specific mutualistic interaction with stable gut-colonizing bacteria. *PLoS Biol* 16: e2005710
- Paone P, Cani PD (2020) Mucus barrier, mucins and gut microbiota: the expected slimy partners? *Gut* 69: 2232–2243
- Patel B, Banerjee R, Basu M, Lenka S, Samanta M, Das S (2016) Molecular cloning of IgZ heavy chain isotype in *Catla catla* and comparative expression profile of IgZ and IgM following pathogenic infection. *Microbiol Immunol* 60: 561–567
- Peng W, Lu DQ, Li GF, Zhang X, Yao M, Zhang Y, Lin HR (2016) Two distinct interferon-gamma genes in *Tetraodon nigroviridis*: functional analysis during *Vibrio parahaemolyticus* infection. *Mol Immunol* 70: 34–46
- Pepi M, Focardi S (2021) Antibiotic-resistant bacteria in aquaculture and climate change: a challenge for health in the Mediterranean area. *Int J Environ Res Public Health* 18: 5723
- Pertea M, Kim D, Pertea GM, Leek JT, Salzberg SL (2016) Transcript-level expression analysis of RNA-seq experiments with HISAT, StringTie and ballgown. *Nat Protoc* 11: 1650–1667
- Portner HO, Peck MA (2010) Climate change effects on fishes and fisheries: towards a cause-and-effect understanding. *J Fish Biol* 77: 1745–1779
- Price MN, Dehal PS, Arkin AP (2010) FastTree 2 – approximately maximum-likelihood trees for large alignments. *PLoS One* 5: e9490
- R Core Team (2019) *R: a language and environment for statistical computing*. Vienna: R Foundation for Statistical Computing
- Rodgers FH, Gendrin M, Wyer CAS, Christophides GK (2017) Microbiota-induced peritrophic matrix regulates midgut homeostasis and prevents systemic infection of malaria vector mosquitoes. *PLoS Pathog* 13: e1006391
- Rogier EW, Frantz AL, Bruno ME, Kaetzel CS (2014) Secretory IgA is concentrated in the outer layer of colonic mucus along with gut bacteria. *Pathogens* 3: 390–403
- Segata N, Izard J, Waldron L, Gevers D, Miropolsky L, Garrett WS, Huttenhower C (2011) Metagenomic biomarker discovery and explanation. *Genome Biol* 12: R60
- Serra CR, Oliva-Teles A, Enes P, Tavares F (2021) Gut microbiota dynamics in carnivorous European seabass (*Dicentrarchus labrax*) fed plant-based diets. *Sci Rep* 11: 447
- Shi Y, Fan Z, Li G, Zhang L, Yue Z, Yan X, Xu A, Huang S (2020) The family of amphioxus chitin synthases offers insight into the evolution of chitin formation in chordates. *Mol Phylogenet Evol* 143: 106691
- Smith ME, Morton DG (2010) 1 – Overview of the digestive system. In *The Digestive System*, Smith ME, Morton DG (eds), 2nd edn, pp 1–18. London: Churchill Livingstone
- Stumpf M, Hu MY, Tseng YC, Guh YJ, Chen YC, Yu JK, Su YH, Hwang PP (2015) Evolution of extreme stomach pH in bilateria inferred from gastric alkalization mechanisms in basal deuterostomes. *Sci Rep* 5: 10421
- Tang WJ, Fernandez JG, Sohn JJ, Amemiya CT (2015) Chitin is endogenously produced in vertebrates. *Curr Biol* 25: 897–900
- Tarnecki AM, Burgos FA, Ray CL, Arias CR (2017) Fish intestinal microbiome: diversity and symbiosis unravelled by metagenomics. *J Appl Microbiol* 123: 2–17
- Tellam RL, Wijffels G, Willadsen P (1999) Peritrophic matrix proteins. *Insect Biochem Mol Biol* 29: 87–101
- Terra WR (2001) The origin and functions of the insect peritrophic membrane and peritrophic gel. *Arch Insect Biochem Physiol* 47: 47–61
- Thomson AB, Chopra A, Clandinin MT, Freeman H (2012a) Recent advances in small bowel diseases: part I. *World J Gastroenterol* 18: 3336–3352
- Thomson AB, Chopra A, Clandinin MT, Freeman H (2012b) Recent advances in small bowel diseases: part II. *World J Gastroenterol* 18: 3353–3374
- Townhill BL, Pinnegar JK, Righton DA, Metcalfe JD (2017) Fisheries, low oxygen and climate change: how much do we really know? *J Fish Biol* 90: 723–750
- Vejnar CE, Moreno-Mateos MA, Cifuentes D, Bazzini AA, Giraldez AJ (2016) Optimized CRISPR-Cas9 system for genome editing in zebrafish. *Cold Spring Harb Protoc* 2016: pdb.prot086850
- Wallace KN, Akhter S, Smith EM, Lorent K, Pack M (2005) Intestinal growth and differentiation in zebrafish. *Mech Dev* 122: 157–173
- Wang P, Granados RR (2000) Calcofluor disrupts the midgut defense system in insects. *Insect Biochem Mol Biol* 30: 135–143
- Wang Z, Du J, Lam SH, Mathavan S, Matsudaira P, Gong Z (2010) Morphological and molecular evidence for functional organization along the rostrocaudal axis of the adult zebrafish intestine. *BMC Genomics* 11: 392
- Wong MH, Mo WY, Choi WM, Cheng Z, Man YB (2016) Recycle food wastes into high quality fish feeds for safe and quality fish production. *Environ Pollut* 219: 631–638
- Xu G, Zhang J, Ma R, Wang C, Cheng H, Gong J, Wang Z, Meng Q (2021) The immune response of plgR and Ig to *Flavobacterium columnare* in grass carp (*Ctenopharyngodon idellus*). *Fish Shellfish Immunol* 117: 320–327
- Yang C, Lim W, Song G (2021) Reproductive toxicity due to herbicide exposure in freshwater organisms. *Comp Biochem Physiol C Toxicol Pharmacol* 248: 109103
- Zhang N, Zhang XJ, Chen DD, Oriol Sunyer J, Zhang YA (2017) Molecular characterization and expression analysis of three subclasses of IgT in rainbow trout (*Oncorhynchus mykiss*). *Dev Comp Immunol* 70: 94–105
- Zhou Y, Zhou B, Pache L, Chang M, Khodabakhshi AH, Tanaseichuk O, Benner C, Chanda SK (2019) Metascape provides a biologist-oriented resource for the analysis of systems-level datasets. *Nat Commun* 10: 1523
- Zhu KY, Merzendorfer H, Zhang W, Zhang J, Muthukrishnan S (2016) Biosynthesis, turnover, and functions of chitin in insects. *Annu Rev Entomol* 61: 177–196